Universidade Estadual Paulista “Júlio de Mesquita Filho”
Instituto de Biociências
Departamento de Ciências Químicas e Biológicas

GENERATION OF *T. cruzi* STRAINS KNOCK-OUT FOR IP6K AND EVALUATION OF THE RESULTING PHENOTYPES

Bryan Etindi Abuchery

Botucatu – SP
July, 2023

Bryan Etindi Abuchery

GENERATION OF *T. cruzi* STRAINS KNOCK-OUT FOR IP6K AND EVALUATION OF THE RESULTING PHENOTYPES

Dissertação apresentada junto ao Programa de Pós-graduação em Ciências Biológicas – Genética do Instituto de Biociências, UNESP, câmpus de Botucatu, como pré-requisito para obtenção do título de mestre em Ciências Biológicas – Genética.

Orientador: Prof. Dr. Marcelo Santos da Silva
Coorientadora: Dra. Simone G. Calderano

Botucatu – SP
July, 2023

FICHA CATALOGRÁFICA ELABORADA PELA SEÇÃO TÉC. AQUIS. TRATAMENTO DA INFORM.
DIVISÃO TÉCNICA DE BIBLIOTECA E DOCUMENTAÇÃO - CÂMPUS DE BOTUCATU - UNESP
BIBLIOTECÁRIA RESPONSÁVEL: ROSEMEIRE APARECIDA VICENTE-CRB 8/5651

Abuchery, Bryan Etindi.
Generation of *T. cruzi* strains knock-out for IP6K and evaluation of the resulting phenotypes / Bryan Etindi Abuchery. - Botucatu, 2023

Dissertação (mestrado) - Universidade Estadual Paulista "Júlio de Mesquita Filho", Instituto de Biociências de Botucatu
Orientador: Marcelo Santos da Silva
Coorientador: Simone Guedes Calderano
Capes: 20202008

1. Chagas, Doença de. 2. *Trypanosoma cruzi*. 3. Proteína 9 Associada à CRISPR. 4. Fosfatos de Inositol. 5. Fenótipo.

Palavras-chave: CRISPR/Cas9; Inositol Pyrophosphates; Pyrophosphorylation; *Trypanosoma cruzi*.

ACKNOWLEDGEMENTS

I would like to express my deepest appreciation to my supervisor, Dr. Marcelo S. da Silva (IQ-USP, Brazil) for the invaluable guidance throughout the entire fellowship period; my co-supervisor Dr. Simone G. Calderano (Butantan Institute, Brazil) and Dr. Bruno Alves Santarossa (Butantan Institute, Brazil) for generating the different lineages used in this study; Dr. Maria Cristina M. Motta (UFRJ, Brazil) for the Electron Microscopy analyses; Dr. Samuel C. Teixeira (UFU, Brazil) and Dr. Eloisa A. V. Ferro (UFU, Brazil) for their input in infection assays and analyses; Dr. Miguel A. Chiurillo (University of Cincinnati, USA) and Dr. Noelia M. Lander (University of Cincinnati, USA) for the CRISPR/Cas9-Riboswitch-Based technology; Dr. Maria Isabel N. Cano (UNESP, Brazil) and Dr. Nilmar S. Moretti (UNIFESP, SP, Brazil) for their guidance. Many thanks to my classmates and laboratory colleagues: Dr. Débora Andrade da Silva, Dr. Thaise L. Teixeira, Vitor L. da Silva (PhD), Arthur O. Passos (MSc), Yete G. Ferri (MSc) for valuable advice, suggestions and moral support. Lastly, I would like to acknowledge my family members, principally my mother and sister for their immense emotional support and for believing in me.

This work was supported by the São Paulo Research Foundation (FAPESP) – processes numbers: 2019/10753-2; 2020/10277-3; 2022/04595-8 and 2020/16480-5; and The Coordination for the Improvement of Higher Education Personnel – Brazil (CAPES).

ABSTRACT

Chagas disease is a neglected tropical disease caused by the protozoan parasite *Trypanosoma cruzi*. There are no effective vaccines and the available treatment options are effective only in the acute phase of the disease but can cause serious side effects on the patients. Thus, the search for the elucidation of molecular pathways that may provide potential targets for drug development is of paramount importance. Inositol pyrophosphates (PP-IPs) – mainly IP_7, and IP_8 – are involved in a wide range of processes in eukaryotes. However, the mechanism of action of these metabolites is not yet fully understood. IP_7 and IP_8 are synthesized by pathways involving the participation of IP6K and PP-IP5K kinases, respectively. Trypanosomatids have an ortholog gene for IP6K but do not have orthologs for PP-IP5K, making them excellent models for studying IP_7. Here, using CRISPR/Cas9 approach, we disrupted single and double alleles of IP6K, generating $IP6K^{-/+}$ and $IP6K^{-/-}$ lineages, respectively. IP6K inactivation causes several morphological effects, such as rounding and wrinkling of the cell body, increased number of glycosomes, and mitochondrial enlargement. Notably, $IP6K^{-/-}$ lineage (double-null) was unable to proliferate for more than 7 days, suggesting that this kinase is essential for this organism. Interestingly, $IP6K^{-/+}$ lineage (single-null) showed a slight cell cycle arrest at G0/G1 phase with no DNA damage (quiescent cells). Moreover, the $IP6K^{-/+}$ lineage showed a high proliferative capacity within the host mammalian cell, suggesting that the quiescent cells observed may be metacyclic forms. Together, our findings suggest that the total loss of IP6K has harmful consequences for *T. cruzi*. However, paradoxically, the disruption of a single allele of IP6K leads to *T. cruzi* being prone to multiplying further inside the host cell, generating a conundrum that we are still trying to understand.

Keywords: CRISPR/Cas9, inositol pyrophosphates, pyrophosphorylation, *Trypanosoma cruzi*.

RESUMO

A doença de Chagas é uma doença tropical negligenciada causada pelo parasita protozoário *Trypanosoma cruzi*. Não existem vacinas eficazes e as opções de tratamento disponíveis são eficazes apenas na fase aguda da doença, mas podem causar efeitos colaterais graves nos pacientes. Assim, a busca pela elucidação de vias moleculares que possam fornecer potenciais alvos para o desenvolvimento de fármacos é de suma importância. Pirofosfatos de inositol (PP-IPs) – principalmente IP_7 e IP_8 – estão envolvidos em uma ampla gama de processos em eucariotos. No entanto, o mecanismo de ação desses metabólitos ainda não é totalmente compreendido. IP_7 e IP_8 são sintetizados por vias envolvendo a participação de IP6K e PP-IP5K quinases, respectivamente. Os tripanossomatídeos possuem um gene ortólogo para IP6K, mas não possuem ortólogos para PP-IP5K, tornando-os excelentes modelos para estudar IP_7. Aqui, usando a abordagem CRISPR/Cas9, interrompemos alelos simples e duplos de IP6K, gerando linhagens IP6K-/+ e IP6K-/-, respectivamente. A inativação do IP6K causa vários efeitos morfológicos, como arredondamento e enrugamento do corpo celular, aumento do número de glicossomos e aumento mitocondrial. Notavelmente, a linhagem IP6K-/- (duplo nulo) foi incapaz de proliferar por mais de 7 dias, sugerindo que esta quinase é essencial para este organismo. Curiosamente, a linhagem IP6K-/+ (single-null) mostrou uma leve parada do ciclo celular na fase G0/G1 sem nenhum dano ao DNA (células quiescentes). Além disso, a linhagem IP6K-/+ mostrou uma alta capacidade proliferativa dentro da célula hospedeira de mamífero, sugerindo que as células quiescentes observadas podem ser formas metacíclicas. Juntos, nossos resultados sugerem que a perda total de IP6K tem consequências prejudiciais para o *T. cruzi*. No entanto, paradoxalmente, o rompimento de um único alelo do IP6K faz com que o *T. cruzi* fique propenso a se multiplicar ainda mais dentro da célula hospedeira, gerando um enigma que ainda estamos tentando entender.

Palavras-chave: CRISPR/Cas9, pirofosfatos de inositol, pirofosforilação, *Trypanosoma cruzi*.

FOREWORD

This document is being presented in English, according to international scientific practice.

ABBREVIATIONS

BER – Base excision repair

BLAST – Basic Local Alignment Search Tool

C – Cytokinesis

Cas9 – CRISPR-associated protein 9

CRISPR – Clustered Regularly Interspaced Short Palindromic Repeats

DAPI – 4′,6-diamidino-2-phenylindole

DIC – Differential interference contrast

DT – Doubling Time

EdU – 5-ethynyl-2'-deoxyuridine

EL – Esmeraldo-Like *T. cruzi* CL Brener haplotype

F – Flagellum

G0 – Quiescent-like state

G1 – Gap 1

G2 – Gap 2

HR – Homologous Recombination

IFA – Immunofluorescence assay

IP6K – Inositol polyphosphate kinase

IP_7 – Inositol heptakisphosphate

IP_8 – Inositol octakisphosphate

K – Kinetoplast

KO – knockout

M – Mitosis

N – Nucleus

NEL – Non-Esmeraldo-Like *T. cruzi* CL Brener haplotype

NER – Nucleotide excision repair

PP-IPs – Inositol Pyrophosphates

S – DNA Synthesis

SEM – Scanning Electron Microscopy

T7 – T7 RNA polymerase

TEM – Transmission Electron Microscopy

γH2A – Phosphorylated histone H2A

LIST OF FIGURES

TABLE OF CONTENTS

1. BACKGROUND

1.1 Inositol Pyrophosphates (PP-IPs)

Phosphate groups are universal biomolecules used in facilitating cell signaling (Wang et al., 2014). These biomolecules determine geometric constraints between protein-protein interactions and ligand-protein interactions, as well as establish specificity through hydrogen and ionic bonding only to specific amino acid residues at physiological pH through their negative charges. This specific signaling is further magnified through interactions that make use of phosphates such as those found placed at various combinations around a six-carbon inositol ring (Wang et al., 2014). *Myo*-inositol (1,2,3,4,5,6-cyclohexanol) is the most abundant inositol and has 5 equatorial hydroxyl groups and one axial (the 2-hydroxyl) and thus is covalently bonded to these phosphate molecules (Barker et al., 2009). From each of the molecules formed, the inositol phosphates (InsPs/IPs), have a characteristic three-dimensional phosphate pattern which encodes a unique set of signaling properties (Barker et al., 2009; Wang et al., 2014; Shears, 2015). Found within this family of signaling molecules, occurs a subgroup that possess functionally significant, "high-energy" diphosphate groups: the inositol pyrophosphates (PP-IPs) (Choi et al., 2007; Fridy et al., 2007; Shears et al., 2017).

PP-IPs are a specialized group of water-soluble molecules characterized by containing one or more high-energy pyrophosphate moieties attached to their inositol ring (Saiardi et al., 2004; Jadav et al., 2013; Cordeiro et al., 2017). Discovered in early 1990s, these biomolecules are so named to differentiate them from their monoester IPs counterparts, and are immensely involved in cellular signaling (Shears, 2018). While the general nomenclature of IPs and PP-IPs has been established, there have been different isoforms of PP-IPs elucidated from different organisms (Mukherjee et al., 2020). Briefly, in mammals, there have been four major types of PP-IPs have been described: 5-diphosphoinositol (1,3,4,6)-tetrakisphosphate (5-PP-IP_4), 1-diphosphoinositol (2,3,4,5,6) pentakisphosphate (1-PP-IP_5 or 1-IP_7), 5-diphosphoinositol (1,2,3,4,6) pentakisphosphate (5-PP-IP_5 or 5-IP_7) and 1,5-bisdiphosphoinositol (2,3,4,6) tetrakisphosphate (1,5-PP2-IP_4 or 1,5-IP_8). Of note, 5-IP_7 is the best characterized inositol pyrophosphate (Mukherjee et al., 2020).

In mammals, a family of three inositol hexakisphosphate kinases isoforms (IP6K1, IP6K2 and IP6K3) have been shown to synthesize 5-IP_7 by adding a phosphate group on the position 5 of the inositol ring (Mukherjee et al., 2020; Saiardi et al., 1999). The IP6Ks have also been shown to generate 5-PP-IP_4 using IP_6 and ATP as precursors. There is another family of kinases (PPIP5K1 and PPIP5K2) that synthesize 1-IP_7 from IP_6 (Choi et al., 2007; Fridy et al., 2007; Shears et al., 2017). Moreover, IP6Ks or PPIP5Ks can phosphorylate 1-IP_7 or 5-IP_7, respectively, to generate 1,5-IP_8, which is usually undetectable under basal conditions (Mukherjee et al., 2020; Saiardi et al., 1999). Also, another class of kinases belonging to the *Nudt gene* family (Diphosphoinositol

Phosphohydrolases) can dephosphorylate the PP-IPs back into their precursor molecules through hydrolysis (Mukherjee et al., 2020). IP6Ks depend on the cellular ATP/ADP ratio that partly explains the higher levels of PP-IPs in anabolic conditions.

In general, the synthesis of IP_5 and IP_6 (precursors of PP-IPs) has been shown to take two routes: the lipid route and soluble route. In the lipid route, PIP_2 (presented in lipidic bilayer) can be cleaved by a phosphoinositide phospholipase C (PI-PLC) to inositol 1,4,5-trisphosphate (IP_3) and 1,2-diacylglycerol (DAG), which are important second messengers (Cocco et al., 2015). While DAG stimulates a protein kinase C (Nishizuka, 1986), IP_3 stimulates an IP_3 receptor to release Ca^{2+} from intracellular stores and can be further metabolized to other soluble inositol phosphates (IPs) by several kinases and phosphatases (Berridge, 2009). The inositol phosphate multikinase (IPMK) has dual 3-kinase/6-kinase activity and catalyzes the conversion of IP_3 into inositol 1,3,4,5-tetrakisphosphate (IP_4) and inositol 1,3,4,5,6-pentakisphosphate (IP_5) (Mukherjee et al., 2020). It also worth noting that inositol triphosphate kinases (IP3Ks) can also use IP_3 as a substrate to synthesize IP_4. IP_5 is then converted into IP_6, also known as phytic acid, by the 2-kinase activity of inositol pentakisphosphate kinase (IP5K or IPPK). Some studies have also shown that ITPK1 is capable of phosphorylating IP_3 to IP_4 and has a bi-directional function that phosphorylate IP_4 to IP_5 and back (Mukherjee et al., 2020; Lee et al., 2020). The soluble routes begin with the formation of 1-IP_3 from inositolphosphoceramide (IPC) by inositol phosphoryl ceramide 1 (IPC1) and further kinase reactions by ITPK1 or starting with the conversion of Glu-6-P to 3-IP1 by INOS1 (IPS) and then a series of kinase reactions catalyzed by ITPK1 or starting with the formation of 1-IP_3 from inositolphosphoceramide (IPC) by Phosphosphingolipids phospholipase C (ISCL) ISC1 and further kinase reactions by ITPK1 (Mantilla et al., 2021a) (a simplified scheme is shown in Figure 1).

1.2 Function and possible modes of action of PP-IPs

In model eukaryotes, the PP-IPs are involved in a wide range of cellular processes, such as apoptosis (Taylor et al., 2012; Nagata et al., 2005; Nagata et al., 2010), tumor growth and metastasis (Rao et al., 2014), fungal pathogenicity (Lev et al., 2015; Kang, 2018; Desmarini et al., 2020), telomere length regulation (Saiardi et al., 2005), homologous recombination (HR) (Jadav et al., 2013), among others.

The involvement of PP-IPs in apoptotic processes was evidenced through the deletion of IP6K, which appears to be involved in the phagophore assembly site, since its depletion led to the reduction of autophagosomes, causing the formation of autophagosome-like structures in abnormal subcellular locations (Taylor et al., 2012; Nagata et al., 2005; Nagata et al., 2010; Deng et al., 2019).

As mentioned, PP-IPs have also been implicated in tumor growth and metastasis, where IP_7 synthesis seems to be a key player in the migration of cancer cells and invasion of and metastasis of tumors both in cell culture and in intact mice (Rao et al., 2014).

PP-IPs in opportunistic pathogen fungi, such as *Cryptococcus neoformans*, have been revealed to be key metabolites essential for fungal metabolic adaptation to the host environment, immune recognition, and pathogenicity (Kang, 2018; Lev et al., 2015; Kang, 2018; Desmarini et al., 2020). However, the specific mode of action has yet to be revealed.

In telomere length regulation, PP-IPs seems to antagonize the functions of the kinases Tel1 and Mec1 (homologs of ATM and ATR), known to regulate telomere length in yeast (Saiardi et al., 2005). Curiously, ATM and ATR also play a prominent role in some DNA repair pathways, such as homologous recombination (HR), in eukaryotes, which include trypanosomatids (Stortz et al., 2017; Marin et al., 2018; Black et al., 2020).

Research studies have shown that the depletion of IP6K1 in mouse embryonic fibroblasts (MEFs) exhibit impaired DNA damage repair via HR (Jadav et al., 2013). IP6K1$^{-/-}$ MEFs showed decreased viability and reduced recovery after DNA damage induction. It was elucidated that cells lacking IP6K1 went into cell-cycle arrest after DNA double-stranded breaks, despite having markers related to DNA repair being recruited to DNA damage sites. This indicated that HR repair was initiated but did not proceed to completion, since these markers persisted as nuclear foci long after drug removal (Jadav et al., 2013; Wang et al., 2014). These findings suggest that IP6K (consequently PP-IPs) should play a key role in HR pathway, a conserved DNA repair pathway of paramount importance for trypanosomatids. However, the mechanism of action of PP-IPs in this pathway still needs to be demonstrated.

To date, most findings demonstrated that not only PP-IPs enhance a central line of communication between signaling and metabolic networks, but also bring out the unusual ability of these molecules to access two distinct modes of action (Wu et al., 2016; Park et al., 2018): (i) the transferring of the β-phosphate group to a previously phosphorylated protein, a process known as non-enzymatic covalent protein pyrophosphorylation (Saiardi et al. 2004; Bhandari et al. 2007); or (ii) the allosteric non-covalent binding to a protein, acting as molecular glue and causing conformational changes (Wilson et al. 2013; Chin et al., 2020; Zhang et al., 2021). Of note, pyrophosphorylation is thought to be enzyme-independent, but it requires the presence of divalent cations, preferably Mg^{2+} (Wu et al., 2016). This posttranslational modification has however proven difficult to detect and has only been visualized so far using radiolabeled PP-IPs in an *in vitro* pyrophosphorylation reaction (Bhandari et al., 2007; Saiardi et al., 2004; Marmelstein et al., 2018; Wu et al., 2016).

1.3 Inositol pyrophosphates (PP-IPs) and *Trypanosoma cruzi*

In trypanosomatids, such as *Trypanosoma cruzi*, the synthesis of PP-IPs follows the classical mammalian lipid route, where the PP-IPs precursors are predominantly derived from membrane phospholipids. Curiously, homologues for PP-IP5K have not yet been found in these parasites, which

would theoretically prevent 1,5-IP_8 synthesis (Cordeiro et al., 2017) (Figure 1). However, a recent study found an isomer of 1,5-IP_8 in *Trypanosoma cruzi* (Mantilla et al., 2021a), which can be explained by two hypotheses: the existence of a divergent kinase able to catalyzes the 1,5-IP_8 synthesis, or an alternative pathway for PP-IPs (5-IP_7 and 1,5-IP_8) synthesis (Cridland and Gillaspy, 2020) not yet elucidated in trypanosomatids. Regardless of which of these hypotheses may be correct, the implications of the 1,5-IP_8 presence in *T. cruzi* have yet to be determined and may suggest prominent roles for PP-IPs.

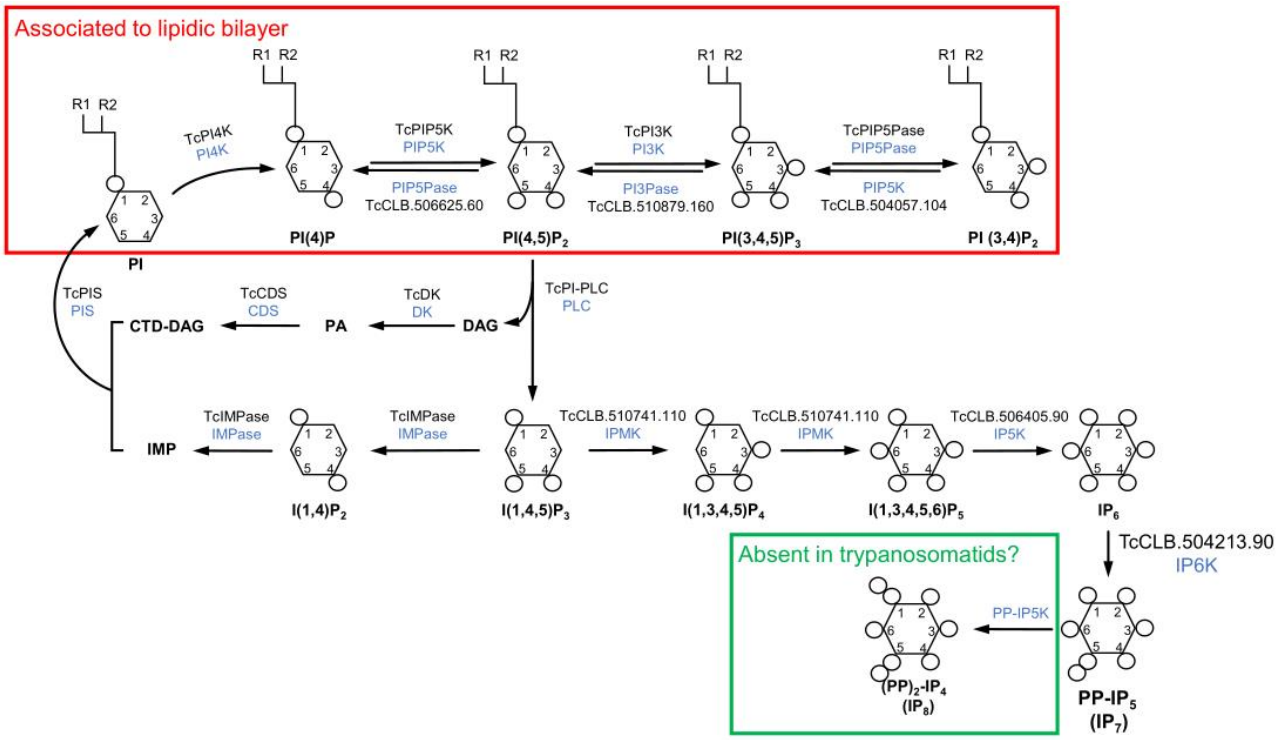

Figure 1. Simplified scheme showing the putative pathway for PP-IPs synthesis in *T. cruzi*. Trypanosomatids apparently do not have orthologs for PP-IP5K, which possibly impair the 1,5-IP_8 synthesis (green highlight). Mammalian enzymes are written in blue. Gene IDs for *T. cruzi* orthologs are in black. PI = Phosphatidylinositol, DAG = diacylglycerol, PA = 4 phosphatidic acid, CTD-DAG = cytoplasmic domain of DAG, IMP = inosine monophosphate, R1 = palmitic acid, R2 = oleic acid. PP-IP_4 synthesis was omitted.

T. cruzi is a single-celled eukaryotic parasite and etiologic agent of Chagas disease, which affect millions of people worldwide, leading to thousands of deaths annually, mainly in Latin America (Khare et al., 2016; Browne et al., 2017). There are no effective vaccines against this disease yet and treatments rely on drugs developed several decades ago, where the risk of significant side effects may be higher than the benefits of treatment (Urbina and Docampo, 2003; Naula et al., 2005; Khare et al., 2016; Browne et al., 2017).

Thus, investigating molecular mechanisms that may result in the identification of targets for the development of more effective chemotherapies against this disease is undoubtedly important. *T. cruzi* belongs to the Excavata supergroup (Adl et al., 2012), and present some striking peculiarities regarding their molecular biology relative to eukaryotic models. Some of these can be highlighted:

T. cruzi organizes the vast majority of its RNA-pol II protein-coding genes into large polycistronic clusters, and nearly all genes lack introns (reviewed in da Silva and Cano, 2017); the canonical non-homologous end joining (cNHEJ) repair pathway is apparently absent (Passos-Silva et al., 2010; Nenarokova et al., 2019); and HR repair pathway is used in ways not fully understood: *e.g.*, HR directs high levels of ionizing radiation resistance in *T. cruzi* (Regis-da-Silva et al., 2006; Garcia et al., 2016), which may have comparisons with HR's role in genome plasticity in *Leishmania* spp. (Genois et al., 2015; Laffitte et al., 2016).

Among the roles related to DNA metabolism attributed to the PP-IPs (Saiardi et al., 2005; Jadav et al., 2013), HR stand out in *T. cruzi* for at least two reasons: First, *T. cruzi* has HR as the most important DNA repair pathway to deal with DNA double-strand breaks (DSBs) (Regis-da-Silva et al., 2006; Garcia et al., 2016; da Silva, 2021) that can arise in different ways during their life cycles since the canonical NHEJ is absent (Regis-da-Silva et al., 2006; Nenarokova et al., 2019). Second, HR plays a crucial role in the genetic exchange, a mechanism that allows the generation of new lineages and, consequently, diversity in these organisms. However, the morphological stage and the environment where this occurs is not well established (Gaunt et al., 2003; Alves et al., 2018; Schwabl et al., 2019). Despite this relevance, little is known about these important pathways and its correlation with PP-IPs in trypanosomatids, with fewer studies having been done to investigate inositol phosphates or pyrophosphates in this parasite (Cestari and Stuart, 2015; Cordeiro et al., 2017; Mantilla et al., 2021; Mantilla et al., 2021b).

Thus, this work aimed to investigate the main functions of PP-IPs in *T. cruzi* (CL Brener). For this, we depleted the IP6K, generating knockout lineages ($IP6K^{-/+}$ and $IP6K^{-/-}$), and investigated the resulting phenotypes. Together, our findings suggest that the total loss of IP6K has harmful consequences for *T. cruzi*. However, curiously, the disruption of a single allele of IP6K leads to *T. cruzi* being prone to multiplying further inside the host cell, a finding that suggests IP6K is related to metacyclogenesis. In future projects derived from this work, we intend to investigate the possible role of PP-IPs in DNA damage repair pathways (with focus on HR), since *T. cruzi* (CL Brener) is a naturally-occurring fused-cell hybrid strain and displays increased levels of RAD51 and BRCA2 transcripts (Alves et. al., 2018). Of note, the results from this work will contribute to a better understanding of the correlation between pyrophosphorylation and DNA metabolism. This knowledge could lead to advances in the treatment not only of Chagas disease, but also of other diseases related to DNA metabolism and PP-IPs, such as cancer (Rao et al., 2015).

2. OBJECTIVES

Main goal

To deplete the kinase IP6K from *T. cruzi* (CL Brener) epimastigotes and evaluate the resulting phenotypes.

Specific goals

To apply the CRISPR-Cas9 system in *T. cruzi* to generate IP6K KO lineages (IP6K$^{-/+}$ or IP6K$^{-/-}$); to confirm the depletion using RT-qPCR; to analyse the growth curves and cell morphology; to investigate the presence of cell cycle arrest and DNA damage; To analyse the infection capacity of the IP6K KO lineages generated.

3. MATERIALS AND METHODS

3.1 Phylogenetic and *in silico* analysis

The amino acid sequences of IP6K from *T. cruzi* (TcCLB.504213.90 – Esmeraldo-Like and TcCLB.506985.60 – Non-Esmeraldo-Like) were downloaded from TriTrypDB (tritrypdb.org/tritrypdb/app) and used to blast for orthologous sequences both in TritrypDB and Protein Databases. Orthologous amino acid sequences were put in one txt file, cleaned and dereplicated using R. The file was used to generate a mapping file consisting of sequence identifiers by organism name and the phyla in which they belonged. The sequences were aligned using Clustal Omega (Sievers et al., 2011) due to size of the fasta file using the command-line program and trimmed to remove misaligned columns using trimAl v1.4.rev15 (Salvador et al., 2009) at a 0.1 gap threshold. The sequences were then re-aligned using MUSCLE v3.8.1551 (Edgar, 2004) to generate a Multiple Sequence Alignment (MSA) file. To infer a phylogenetic tree, RAxML-NG (Randomized Axelerated Maximum Likelihood – Next Generation), a program for sequential and parallel Maximum Likelihood (Alexey et al., 2019) based inference of large phylogenetic trees was used. RAxML-NG infers Maximum Likelihood based on iteratively performing integrated series of Subtree Pruning and Regrafting (SPR) events, which allows it to quickly for the best-known ML tree (Alexey et al., 2019) using base frequencies provided by the best fitting model (Jones-Taylor-Thorton, JTT).

Briefly, the Multiple Sequence Alignment (MSA) is read to ensure it doesn't contain sites of undetermined characters, sequences with undefined characters, duplicate taxon names or any other format errors (Alexey et al., 2019). A tree is then inferred using JTT-GAMMA (partitioned analysis) default parameters by performing 20 tree searches using 10 random and 10 parsimony-based starting trees. The best-scoring topology tree topology is picked and then a standard non-parametric bootstrapping by re-sampling alignment columns and re-inferring the tree for each bootstrap replicate (100 replicates) of the MSA is done to get accurate support values (Alexey et al., 2019). By default,

RAxML-NG performs MRE-based bootstrapping test after every 50 replicates and terminates once the diagnostic statistics drops below the computational cutoff value (Alexey et al., 2019). BS (bootstrap) support values are then mapped onto the best-scoring/best-known ML tree and a Tree Likelihood Evaluation is finally done to compute the likelihood of a given fixed tree topology by optimizing model and/or branch length parameters on that fixed tree (Alexey et al., 2019).

The run was performed in UNESP's system grid server, (Intel(R) Xeon(R) CPU E5-2680 v4 @ 2.40GHz, 28 cores, 125 GB RAM) consisting of parallelization scheme autoconfig: 3 worker(s) x 9 thread(s) that took 395953.532 seconds to run. Consumed energy was 24244.379 Wh (= 121 km in an electric car, or 606 km with an e-scooter). The tree was visualized through Interactive Tree of Life v5 (Ivica Letunic, 2021).

The IP6K nucleotide sequences downloaded from TriTrypDB were used during *T. cruzi* genome editing analyses. The tools available on the TritrypDB (*e.g*., blast, sequence retriever, etc.), and tools available at leishGEdit website (http://www.leishgedit.net/) were used to prepare the gene knockout toolkit. The sgRNAs and fragments of donors DNA were designed using the tools available on TritrypDB (tritrypdb.org), leishGEdit (leishGEdit.net), and Snapgene viewer (snapgene.com), following the methodology described by Beneke et al. (2017) and Costa et al., 2018 (Beneke et al., 2017; Costa et al., 2018).

3.2 Cultivation of *T. cruzi* (CL Brener strain) epimastigotes

Epimastigote forms of *T. cruzi* (CL Brener strain) were used to carry out most of the assays proposed here. *T. cruzi* epimastigotes were cultured at 28 °C in liver-infusion tryptose (LIT) medium supplemented with 10% fetal bovine serum and 1% (v/v) antibiotic solution (streptomycin/penicillin). The *T. cruzi* epimastigotes lineages containing the T7/Cas9 construct (T7/Cas9) and the lineages generated ($IP6K^{-/+}$ and $IP6K^{-/-}$) were cultivated in the same aforementioned medium, additionally supplemented with the respective drugs: 100 $\mu g.mL^{-1}$ G418 sulfate for T7/Cas9; 10 $\mu g.mL^{-1}$ blasticidin for $IP6K^{-/+}$; and 10 $\mu g.mL^{-1}$ blasticidin for $IP6K^{-/+}$ + 5 $\mu g.mL^{-1}$ puromycin for $IP6K^{-/-}$.

3.3 Growth curves

For the growth curves, fresh cultures of *T. cruzi* (CL Brener) epimastigotes were started at a concentration of 2.10^6 $cells.mL^{-1}$ and counted daily during 7 days. The counting was done using a Neubauer chamber. The final concentration was given by the following formula: $\bar{x}\, quadrants.dilution^{-1}.10^4$. The growth curves were made in triplicates and the standard deviation was estimated through the mean of the concentration values for each day.

3.4 Generation of *T. cruzi* lineages KO for IP6K using CRISPR-Cas9 system

These lineages were generated in collaboration with Dr. Simone G. Calderano (Butantan Institute) using the *T. cruzi* CRISPR/Cas9 approach developed by Costa et al., 2018 and Beneke et al., 2017 (Beneke et al., 2017; Costa et al., 2018).

Donor DNA and 'sgRNA' amplification

The donor DNA amplification was performed through PCR using Phusion High-Fidelity PCR Master Mix (Thermo Fischer) according to the manufacturer's instructions. Primers were designed with 30 bp in the 5' region for homologous recombination and another 20 bp complementary to the plasmids. The donor DNA for KOs was amplified from plasmids pT_puro or pJET_new_blast given as a gift by Dr. Eva Gluenz (University of Glasgow, UK).

The amplification of the DNA responsible for sgRNA transcription ('sgRNA') was carried out in a final reaction of 20 µL according to the manufacturer's instructions (Phusion High-Fidelity PCR Master Mix - Thermo Fischer) using 2 µM of each primer, as described by Beneke et al., 2017 (Beneke et al., 2017). The "Eukaryotic Pathogen CRISPR guide RNA/DNA Design Tool" (http://grna.ctegd.uga.edu/) was used to define the 20-base pairs sequence (protospacer) of the 'sgRNA'. This tool generates several specific sequences that have the PAM motif (5'-NGG-3') for the region to be cleaved, eliminating the possible sequences that would cause unspecific breaks (off-targets).

Prior to transfection, the PCR products were purified on silica columns (QIAquick PCR purification Kit – Qiagen). In the same column, the donor DNA and sgRNA PCR products were purified. The DNA was eluted in 50 µL of TE (10 mM Tris, 1 mM EDTA) previously filtered on a 0.22 µm nylon membrane.

Transfection and clone selection

Two parasite samples were used during transfection (one used as a control and the other for IP6K KO) contained 10 mL of the exponentially growing *T. cruzi* epimastigotes T7/Cas9 lineage (1.10^7 parasites.mL^{-1}). These samples were washed in PBS (137 mM NaCl, 2.7 mM KCl, 10 mM Na_2HPO_4 and 2 mM KH_2PO_4, pH 7.4) and resuspended in 350 µL transfection buffer (120 mM KCl, 0.15 mM $CaCl_2$, 2 mM EDTA, 10 mM K_2HPO_4/KH_2PO_4, 25 mM HEPES, 5 mM $MgCl_2$). One sample containing parasites were transferred to a 0.2 cm cuvette together with the purified PCR products (for IP6K KO). The other one received the same treatment but was added TE buffer instead of PCR products (control). Amaxa Nucleofector IIb (Lonza) was used to perform electroporation according to the manufacturer's instructions. Then, each parasite sample were placed in 5 mL of culture medium and incubated at 28 °C for 24 h.

The day after electroporation, the IP6K KO sample was split into 3 flasks and, subsequently, IP6K KO samples and the control received the needed selection antibiotics (puromycin, blasticidin and/or G418 sulfate). The parasites were incubated at 28 °C in the presence of 5% CO_2. The selection of the polyclonal population was achieved ~14 days after transfection, when no live cells were found in the control group. The monoclonal population was obtained from the polyclonal population after limiting dilution. Of note, the double-null ($IP6K^{-/-}$) lineage was obtained in the same way as described, however using the single-null ($IP6K^{-/+}$) lineage as background.

3.5 Genomic DNA (gDNA) extraction and PCRs

5 mL of epimastigote *T. cruzi* lineages ($IP6K^{-/-}$, $IP6K^{-/+}$, and T7/Cas9) in exponential phase (2.10^7 cells.mL^{-1}) were collected by centrifugation (1600 *g* for 5 min), washed twice in PBS, re-suspended in 4 mL of Lysis solution (200 mM Tris, 10 mM EDTA-pH 8.0, 50 µg.mL^{-1} proteinase K, and 0.5% SDS), and incubated over night at 37 °C. Then, 2.1 mL Phenol (half the total volume) was added and the solution mixed. Next, 2.1 mL of chloroform was added into the solution which was then mixed and centrifuged (1600 *g* for 10 min). The aqueous phase (top phase) was collected and transferred to a clean tube. RNase A (10 µL from the stock 20 mg/mL) was added and incubated at 37 °C for 30 min. Phenol/chloroform/isoamyl alcohol (25:24:1) v/v was added and the solution was mixed gently. The solution was centrifuged again, and the top phase collected into another tube. The gDNA was precipitated by the addition of 30 mM Sodium acetate and twice volume of 100% ethanol. The gDNA containing solution was gently mixed and incubated at -20 °C for 30 min. The gDNA was collected, washed using 70% ethanol (v/v) and solubilized into 1 mL TE solution (10 mM Tris, 1 mM EDTA, pH 8.0). The gDNA samples were stored at 4 °C. The IP6K KO were analysed by standard PCRs (using primers previously designed). For the preparation of the scientific article to be published, IP_7 depletion will be evaluated by PAGE or HPLC coupled with LC-MS/MS, as described (Cordeiro et al., 2017).

3.6 Reverse Transcription quantitative Polymerase Chain Reaction (RT-qPCR)

Total RNA was isolated from 50 mL of epimastigote *T. cruzi* lineages (WT, T7/Cas9, and $IP6K^{-/+}$), each of them in exponential phase (2.10^7 cells.mL^{-1}), using TRIzol (Thermo Fisher Scientific) according to the manufacturer's instructions. RNA integrity was checked by gel electrophoresis and through the Qubit Fluorometer 3.0 Fluorometer analyses (Thermo Fisher Scientific). Two micrograms of total RNA from each individual sample were used for cDNA synthesis using the iScript cDNA Synthesis Kit (BioRad), according to manufacturer's instructions and the previously described protocol (de Waal et al. 2008). The RT-qPCR assays were carried out using the RealQ Plus 2x Master Mix Green (Ampliqon), based on the protocol previously described (de Castro-Assis et al.,

2018) with slight modifications. All RT-qPCRs were performed in 20 µL reactions and cycle threshold (Ct) values for WT, T7/Cas9, and IP6K$^{-/+}$ were obtained in a ViiA 7 Real-Time PCR system (Applied Biosystems) using default settings. The relative gene expression data were analysed using the $2^{-\Delta\Delta CT}$ method as previously described (Livak and Schmittgen 2001). Due to its constitutive expression among all groups analyzed, glyceraldehyde-3-phosphate dehydrogenase (GAPDH) mRNA levels were used as endogenous control. Samples from the control group (T7/Cas9) were normalized to an arbitrary value of 1. The data were expressed as means of fold change over control (normalised expression).

3.7 DNA Content Analysis

The DNA content analyses were accomplished by flow cytometry. *T. cruzi* lineages (IP6K$^{-/-}$, IP6K$^{-/+}$, and T7/Cas9) predominantly in exponential phase (2.10^7 cells.mL^{-1}) were collected by centrifugation (1000 *g* for 5 min). A total of 5 mL (1.10^8 cells.mL^{-1}) were used for each sample. Each *T. cruzi* sample cells were collected by centrifugation (1600 *g* for 5 min) and washed twice using PBS, and fixed/permeabilized with 70% cold ethanol overnight at 4 °C. The pellet containing cells was washed once with PBS and resuspended in 500 µL of PBS containing 10 µg.mL^{-1} of Propidium Iodide (PI) and 100 µg.mL^{-1} of RNase A. After 45 min of incubation at 37 °C, the cells were analyzed using BD Accur C6 Flow Cytometer (BD Biosciences).

3.8 Immunofluorescence Assay (IFA) of IP6K HA-tagged

During an internship abroad held in the laboratory of Dr. Noelia Lander (University of Cincinnati, OH, USA), IP6K from *T. cruzi* (CL Brener) was Hemagglutinin (HA)-tagged in the C-terminal region. This lineage was generated as part of the procedure for application of the CRISPR/Cas9-Riboswitch-based method (Lander et al., 2020). In this dissertation, we chose to omit the CRISPR/Cas9-Riboswitch-based method, as it is still in the standardization phase. However, the generated HA-tagged IP6K lineage was used in IFA assays to identify the subcellular localization of IP6K. Of note, the C-terminal HA-tagged lineage was generate in the same way as described for the generation of *T. cruzi* lineages KO for IP6K using CRISPR-Cas9 system (item 3.4.1), where the DNA donor contained the resistance gene and 3xHA sequences to be inserted at the C-terminal.

500 µL of C-Terminal HA-tagged *T. cruzi* epimastigotes in early exponential phase (1.10^7 cells.mL-1) were collected by centrifugation (1000 *g* for 7 min), washed once in PBS (1000 g for 5 min) before 150 µL of the same PBS was used to re-suspend cells. After 2 min, 50 µL of 16% paraformaldehyde (diluted in PBS) was added adjusting the final concentration of PFA to 4% in pH 7.4 PBS and cells solution. The cells were incubated for 1 h at room temperature. Preparing coverslips for each IFA performed, coverslips were washed with 70% ethanol before they were dried

with Kimwipe. 15 µL of 1 mg.mL-1 Poly-L-Lysine (PLL) solution was put on a piece of parafilm attached to a glass plate using the back of forceps (one drop for each coverslip) and then the coverslips were gently lowered using delicate forceps and gently pressed to cover the entire coverslip with PLL solution. The clean side of the coverslip was labeled with a small asymmetrical letter on the edge to differentiate the PLL/cell side up from down and then incubated for 20 min. DI water was used to wash the coverslips over a waste receptacle and dried them by touching on a Kimwipe on their non-cell side and laying on a new parafilm facing PLL/cell-side up.

200 µL of cells (gently flicked to resuspend them) were added onto the coverslips and gently distributed cells using the pipette tip without touching the PLL when dispensing or moving the culture over the coverslip. Coverslips were covered with a plastic lid to protect them from dust and left at RT for 20 minutes. Using delicate forceps and an excess of cells was removed by touching the sides of the slip on a kimwipe. The covers were placed in a used clean 12-well plate (lid labeled) containing 1 mL of PBS pH 7.4 (1 coverslip per well) with the cells facing upwards for a wash. The PBS was poured off by inverting the plate on the sink (first slowly then more forcefully). This wash was repeated twice more before the wells were refilled with 1 mL of PBS and then checked under a microscope to see if the cells are attached to the coverslip. Slow plate movements were used to check if the cells were attached or floating around.

The PBS was removed from the wells using 1 mL pipette and then the parasites were permeabilized using 1 mL of 0.1% Tritón-X-100 in PBS for 5 min. Triton was removed by inverting the plate on the sink and the cells washed 3 times with 1 mL PBS pH 7.4. 1 mL of blocking solution (50 mM NH_4Cl, 3% BSA, 5% Normal Goat Serum – NGS, 1% fish gelatin in PBS pH 7.4) was added and the cells left for 4 ºC overnight. 15 µL of Mouse anti-Hemagglutinin (anti-HA) (primary antibody), diluted in 1% BSA in PBS pH 8.0 (1:200) was placed onto a strip of parafilm attached on a flat-surfaced glass block whence the coverslips were placed on top of the antibody drops (cells facing downwards). The setup was covered in a makeshift humid chamber (to prevent the cells from drying out) and left at RT for 1 h. The coverslips were returned to the 12-well plate (cell side upwards) and washed 3 times with 1 mL of 1% BSA solution in PBS for 5 min, shaking slowly (at speed 3) for each wash. The same procedure was repeated for the secondary antibody, whereby 15 of µL Donkey Anti Mouse (DAM) 488 (Alexa 488, Dilution 1:500 (already diluted 1:2 with Glycerol so that the final dilution was 1:1000) was used for incubation away from light. After 1 hour, the cells were washed twice with 1 mL of 1% BSA solution in PBS for 5 min, shaking slowly (at speed 3) for each wash and then once with 1 mL of PBS pH 8.0.

Glass slides were prepared by washing them with 70% ethanol and dried using kimwipes. 5 µL of gel mounting media containing DAPI (5 $\mu g.mL^{-1}$) was placed on labeled slides and then the coverslips were put on top of the drop of mounting media (cells facing down). The edges of the coverslips were sealed on slides using gently applied nail polish. To avoid bleaching of the signal,

the slides from this point are handled in the dark and stored at 4 ºC for up to one week or at -20 ºC for longer storage. Images were acquired using a Confocal Microscope, at the University of Cincinnati Children's Hospital.

3.9 IFA – FKN pattern analyses

Some cell cycle phases of trypanosomatids are easily distinguishable by labeling their DNA-containing organelles (nucleus and kinetoplast) and flagellum. *T. cruzi* lineages (IP6K$^{-/-}$, IP6K$^{-/+}$, and T7/Cas9) predominantly in exponential phase (2.10^7 cells.mL^{-1}) were collected by centrifugation (1000 *g* for 5 min), washed twice with PBS, fixed for 10 min with 4% sterile paraformaldehyde (Merck, Germany) diluted in PBS, and added into a 0.1% poli-L-lysine pre-treated slides (Knittel Glaser). The slides were incubated for 5-10 minutes to allow the parasites to dry on the slide. The slides were permeabilized with 0.1% Triton X-100 diluted in PBS for 5 min and then briefly washed by "squirting" PBS on the slides. Anti-flagellum (primary antibody) developed in mouse (da Silva et al., 2013) was diluted in 4% BSA solution (1:10) and added onto the slide, being incubated overnight at 4 °C to minimize chances of non-specific interactions. The slides were carefully washed with PBS before the secondary antibody (Alexa Fluor 555 anti-mouse IgG diluted in 4% BSA - 1:1000) was added and incubated for 2 h at 4 °C away from light. Then, the slides were washed carefully with PBS and left to dry out for few minutes. 5 µL of VectaShield containing DAPI (4′,6-diamidino-2-phenylindole) (Vector) was added onto the slides and a coverslip was mounted. The slides were fixed with nail polish before being observed under a fluorescence microscope. Images were acquired using the fluorescent microscope (Nikon Eclipse 80i) with 100x oil attached to a mercury lamp and a digital camera (Nikon DS-F1i).

DAPI-flagellum-stained exponentially growing epimastigotes were examined to observe the pattern of the flagellum (F), nuclei (N), and kinetoplast (K). The following profiles were measured: 2F2K2N, 2F2K1N, 2F1K1N, 1F1K1N, and others (aberrant cells, i.e., profiles that do not fall within those pre-established).

3.10 IFA – DNA damage analyses

DNA damage can be distinguished by signaling and activating important players involved in DNA damage response, such as γH2A. To investigate the presence of DNA damage, we used an α-γH2A antibody provided as a gift by Dr. Richard MacCulloch (University of Glasgow, UK). As positive control [C(+)], T7/Cas9 lineage was incubated with 500 µg.mL^{-1} phleomycin (InvivoGen) for 2 h. As negative control, T7/Cas9 lineage was processed replacing α-γH2A by PBS. *T. cruzi* lineages [IP6K$^{-/+}$, T7/Cas9, C(+) and C (–)] in exponential phase (1.10^7 cells.mL^{-1}) were collected by centrifugation (1000 *g* for 5 min), washed twice with PBS, fixed for 10 min with 4% sterile paraformaldehyde (Merck,

Germany) diluted in PBS, and added into a 0.1% poli-L-lysine pre-treated slides (Knittel Glaser). The slides were incubated for 5-10 min to allow the parasites to dry on the slide. The slides were permeabilized with 0.1% Triton X-100 diluted in PBS for 5 min and then briefly washed by "squirting" PBS on the slides. Anti-γH2A antibody (primary antibody) developed in rabbit was diluted in 4% BSA solution (1:500) and added onto the slide, being incubated overnight at 4 °C. The slides were carefully washed with PBS before the secondary antibody (Alexa Fluor 555 anti-rabbit IgG diluted in 4% BSA - 1:1000) was added and incubated for 2 h at 4 °C protected from light. Then, the slides were washed carefully with PBS and left to dry out for few minutes. 5 µL of VectaShield containing DAPI (4′,6-diamidino-2-phenylindole) (Vector) was added onto the slides and a coverslip was mounted. The slides were fixed with nail polish before being observed under a fluorescence microscope. Images were acquired using the fluorescent microscope (Nikon Eclipse 80i) with 100x oil attached to a mercury lamp and a digital camera (Nikon DS-F1i).

3.11 EdU incorporation assays and 'click' chemistry reaction

Exponentially growing (2.10^7 cells.mL^{-1}) *T. cruzi* epimastigotes lineages (IP6K$^{-/+}$ and T7/Cas9) were incubated with 200 µM 5-ethynyl-2'-deoxyuridine (EdU) (ThermoFisher Scientific) for different time periods (ranging from 1h to 3.5 h) at 28 °C. The parasites were then harvested (~ 2.10^7 total cells) by centrifugation at 1300 *g* for 5 min, washed twice in PBS, fixed for 10 min with 4% sterile paraformaldehyde (Merck) diluted in PBS, washed twice, and re-suspended in 50 µL of PBS. Then, 25 µL of the cell suspension was loaded onto 0.1% poly-L-lysine pre-treated slides (Knittel Glaser) and permitted to dry. The slides were permeabilized with 0.1% Triton X-100 diluted in PBS for 5 min and then briefly washed by "squirting" 1X PBS on the slides. To detect incorporated EdU, we used 50 µL of Click-iT EdU detection solution for 1 hour protected from light. This solution is composed by 3 mM $CuSO_4$ (Sigma-Aldrich), 5 mM Alexa fluor azide 488 (ThermoFisher Scientific), and 100 mM $C_6H_8O_6$ (ascorbic acid) (Sigma-Aldrich) diluted in PBS (for details about EdU procedure, see (Salic and Mitchison, 2008). Finally, the cells were washed twice with PBS. Vectashield containing DAPI (Vector) was used as an anti-fade mounting solution and to stain nuclei and kinetoplast DNA. Images were acquired using the fluorescent microscope (Nikon Eclipse 80i) with 100x oil attached to a mercury lamp and a digital camera (Nikon DS-F1i). Images were further analyzed using ImageJ software (National Institutes of Health) to count the numbers of EdU-positive cells relative to the total cells. The percentage of parasites in cytokinesis and mitosis were calculated for each group relative to the total number of DAPI-positive parasites. When necessary, images were superimposed using NIS elements software (Nikon).

3.12 Cell cycle analysis

The profile 2F2K2N was used to estimate the percentage of cells in cytokinesis (C). Using this parameter for the all samples analized, we were able to estimate the duration of cytokinesis according to the Williams Equation (Williams, 1971):

$$x = \frac{ln(1-y/2)}{-\alpha},$$

where x is the cumulative time within the cycle until the end of the stage in question, y is the cumulative % of cells up to and including the stage in question (expressed as a fraction of one unit), and α is the specific growth rate.

To estimate the G2+M phases length, we added EdU in the medium containing exponential growing promastigotes and collected samples every 15 min, proceeding with 'click' chemistry reaction, until a parasite containing two EdU-labeled nuclei (2N2K) was observed (this time corresponds to the length of G2+M phases). The difference between this value and the duration of mitosis previously calculated corresponds to G2 phase duration.

To estimate the S-phase duration, we measured the proportion of cells EdU-labeled after 1 h EdU pulse. The S-phase duration was estimated according to the Stanners and Till Equation (Stanners and Till, 1960):

$$S = \frac{1}{\alpha} ln\left[L + e^{\alpha(Z)}\right] - (Z + t),$$

where *L* is the proportion of cells exhibiting EdU-labeled nuclei, α = ln 2.T^{-1} (*T* = doubling time, expressed in hs), Z = G2 + M + cytokinesis, and *t* is the duration of the EdU pulse in hours (h).

Finally, the duration of G1 phase was estimated by the difference between the doubling time (dt) and the sum of the other phases (S+G2+M+C). Of note, all these calculations were made with the help of the online software CeCyD, available at the address cecyd.vital.butantan.gov.br/ (da Silva et al., 2020).

3.13 Quiescent (dormant) cells analysis – Edu-negative selection assay

We developed a pioneering method to quantify cells not committed to the cell cycle (quiescent – dormant cells). This method consists of performing an Edu incorporation for a long period (close to the doubling time) and measuring the cells that were not able to uptake EdU (EdU-negative selection).

Exponentially growing (2.10^7 cells.mL^{-1}) *T. cruzi* epimastigotes lineages (IP6$K^{-/+}$ and T7/Cas9) were incubated with 200 µM EdU (Thermo-Fisher Scientific) for 8 h at 28 °C. For each sample, an equivalent was prepared that was not incubated with EdU. Each sample was collected by centrifugation (900 *g* for 5 min), washed twice using PBS, and fixed/permeabilized with 70% cold ethanol overnight at 4 °C. The samples were vortexed, centrifuged (900 *g* at 4 °C for 5 min), washed

with PBS and incubated with 100 µL of Click-iT EdU detection solution (3 mM $CuSO_4$, 100 mM ascorbic acid, and 5 mM Alexa fluor azide 488 diluted in PBS) for 1 h protected from light. The samples were then washed one more time with PBS and resuspended in 500 mL of PBS. The cells were both analyzed in suspension using a flow cytometer (BD Biosciences) and added onto microscope slides to be analyzed under a fluorescence microscope.

3.14 Infections assays

T. cruzi epimastigotes lineages ($IP6K^{-/+}$ and T7/Cas9) were differentiated into metacyclic (infective) forms using Grace's Insect Tissue Culture Medium (GMA) supplemented with 10% fetal bovine serum, according to the protocol previously described (Sullivan, 1982). Next, the metacyclic forms were used to infect Vero cells at a multiplicity of infection (MOI) 50:1 for 1 h in 2% DMEM. After 6 days, the released TCTs (tissue-culture cell-derived trypomastigotes) were collected by centrifugation and labeled using the CellTrace CFSE Cell Proliferation Kit, according to manufacture instructions (Thermo Fisher Scientific). Briefly, parasites were incubated for 20 min at 37 °C with 10 mM CFSE in PBS buffer. The excess of CFSE was quenched with 2% DMEM for 5 min. After that, cells were centrifuged at 3,000 *g* for 10 min and resuspended with 5 volumes of 2% DMEM. Infection was performed using HeLa cells (protected from light) at a MOI 50:1 for 1 h in 2% DMEM. Afterwards, cells were washed five times with PBS and re-incubated in 2% DMEM for an additional 72 h. Finally, the cells were washed, trypsinizad, collected by centrifugation, washed again and fixed with 4% PFA at 4 °C until the fluorescence reading using the FACSCalibur flow cytometer (Benckton-Dickson). Minimum 10,000 events were measured for each sample. The raw data (FCS files) were analyzed using the FlowJo VX software.

3.15 Statistics and reproducibility

GraphPad Prism 9.0.0 package (GraphPad Software, Inc.) was used for statistical analysis. All datasets were checked for normal distribution using a Shapiro–Wilk normality test. Significant differences between groups were identified using two-tailed Student’s t-test (paired or unpaired, as appropriate). Comparisons of more than two groups were performed with one-way ANOVA followed by Student–Newman–Keuls test. Data are represented as mean ± SEM (standard error of the mean).

4. RESULTS AND DISCUSSION

4.1 IP6K presents slight conservation among eukaryotes

To investigate the conservation level of IP6K among different eukaryotes, we carried out deep *in silico* analyses (Figure 2). Phylogenic trees were inferred using RAxML-NG’s Maximum Likelihood

approach whereby 706 amino acid sequences were analyzed each representing select eukaryotic organisms. The clear classification between members of a monophyletic groups posits a difference in different IP6K families in different species all performing possible similar functions (orthologs), showing a divergent physiological evolution. Results from the NCBI ortholog tblastx search of *T. cruzi* CL Brener (TcCLB.504213.90) show that the *T. cruzi* (CL Brener strain) has an E-value of 0.0 and 99.73% gene identity with *T. cruzi* (Y strain), E-value of 2e-82 and 56.27% gene identity with *Trypanosoma brucei* TREU927 and an E-value of 2e-60 and 47.62% gene identity with *Leishmania donovani*.

Data from BLAST search suggests that TcIP6K, although sharing similar functions with human IP6K isoform 1 and 2, may have diverged from a common ancestor (orthology) about ~2 billion years ago (inferred from % similarity scores as suggested by Pearson, 2013). IP6K is a biomolecule found in all eukaryotic cells (Shah et al., 2017), having first been described in *Dictyostelium discodium* more than 20 years ago. The IP6Ks is constituted in the larger Inositol Polyphosphate Kinase family (IPK-Pfam PF03770), which also encompases IP3Ks, ITPKs and IPMKs (Saiardi et al., 1999; Saiardi et al., 2004; Wang et al., 2014). All these kinases share a similar PxxxDxKxG catalytic motif and whose phylogenetic analyses have proposed that they all arose from a primordial IP6K ancestor (Bennett et al., 2006; Minini et al., 2020).

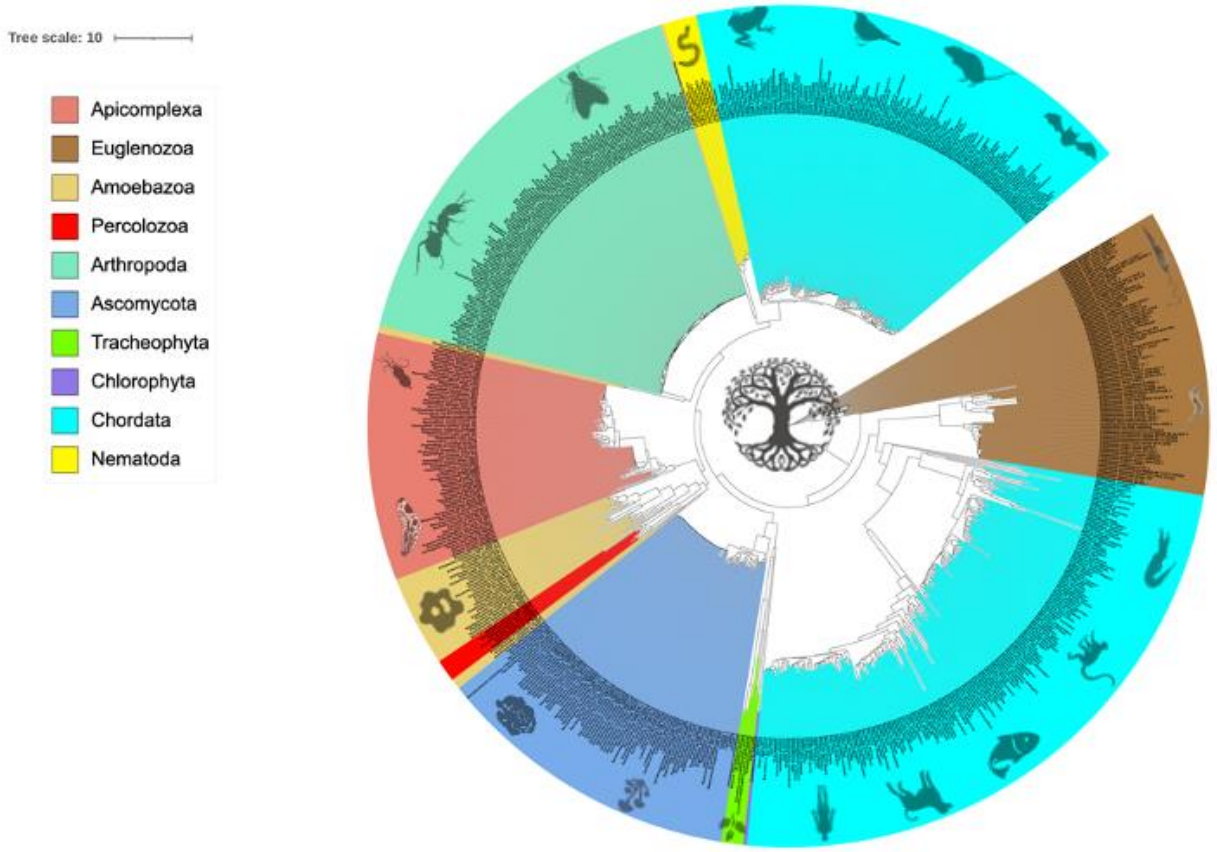

Figure 2. Phylogenetic analyses of IP6K. IP6K phylogenetic analysis of 706 representative sequences constructed on Maximum Likelihood with "JTT+G" matrix rate (LogLikelihood: -799230.272547) and 100 bootstraps reveals that IP6K shows extensive variability among eukaryotes, raising orthologs in members of the same family and considerable conservation (although low) among closely related eukaryote families.

Wang et. al., 2014 have proposed that the primordial IP6K ancestor diverged into different members of the IPK family through compression of its active site, noting that the original IP6K substrate (IP_5/IP_6) is highly polar and substantially larger than the substrates of the descendant kinases: IP_3, phosphorylated by IP3K at the 3-OH and IP_4 and IP_5 which are both phosphorylated by IPMK (Wang et al., 2014). The theory originates from the view that native catalytic activity of enzymes that diverged from promiscuous progenitors generally have smaller substrates whose polarities remain unchanged (Khersonsky et al., 2010). IP6K has a large "open clamshell" geometry whereby one jaw is represented by a long 3_{10} helix while the other is represented by a pair of α-helix (Wang et al., 2014). This makes it possible for the large IP_6 to interact with the 3_{10} helix and both α-helices in the substrate pocket whereas IP_3 has to be rotated 55^0 closer to the α-helices so as to provide its interaction with IP3K in its substrate pocket.

Studies of substrate-bound structures of IP6Ks, including *Homo sapiens* IP6Ks and *Entamoeba histolytica* IP6K, have a vestigial IP3K activity demonstrated by non-overlapping substrate orientations which insert hydrophobic patches on the α-helices enhancing separate IP3K activity that does not affect IP6K activity (Wang et al., 2014). The *E. histolytica* homologue phosphorylates the 6-OH of IP_3, an IPMK-like activity. These changes in orientations of substrates may be used to explain retention of IP6K activity in inositol triphosphate kinase 1 (ITPK1) and inositol triphosphate kinase 2 (ITPK2), especially in plants, whose 5PP-IP_5 is synthesized by these ITPKs (Wang et al., 2014). This theory would perhaps explain why TcIP6K (732 aa), from a divergent organism, is larger than human IP6K (426 aa) and *E. histolytica* IP6K (270 aa).

Among the conserved elements, the IP6K domains in *E. histolytica* identified as N- and C-domains comprise of a similar ATP domain in both IPMK and human IP3K (Wang et al., 2014). The N- terminal lobe in *E. histolytica* IP6K was determined from residues 28-91 consisting of 3 antiparallel β-strands. The β1 and β2 strands are connected by two helices; α1, and α2. Thus, as shown by this organism, it is possible that the original evolutionary trajectory was to favor the multifunctionality of IP6K, whose duplication event may have led to the consolidation of the α-helices and atrophy of other helices in substrate binding region, leading to a gain of function and retention of positional promiscuities in other kinases (Wang et al., 2014).

Next, an alignment was done to compare IP6K amino acid residues from *T. cruzi*, *E. histolytica* and *H. sapiens*. This made it possible to establish the order of different α-helices and β-strands, especially those around the substrate pocket and IP_6 anchoring/binding. The alignment also facilitates the composition of TcIP6K topology so as to visualize interaction of different β-strands and

α-helices in 2D. Additionally, our findings suggest low conservation of IP6K orthologs among distantly related eukaryotes using Swissmodel homology-modelling server (E-value of 1e-07 and 12.23% identity and 3e-18 and 15.01% identity relative to *E. histolytica* IP6K and human IP6K2 respectively) (Figure 3).

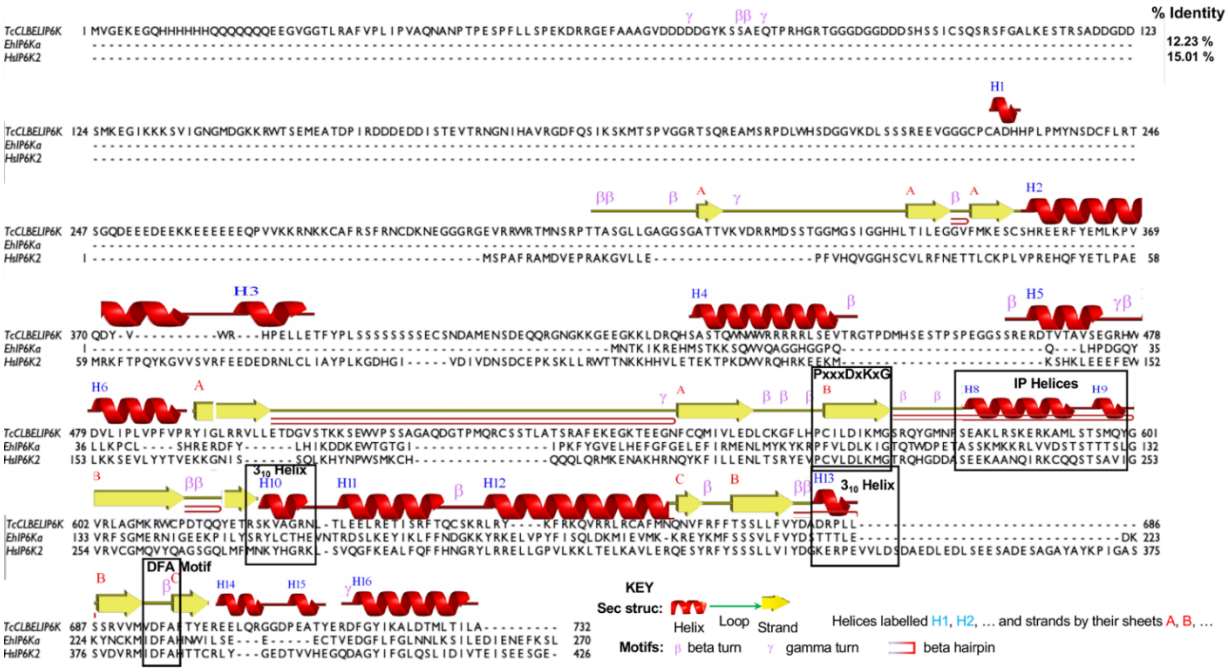

Figure 3. Alignment comparison among *T. cruzi* IP6K, *E. histolytica* IP6K and human IP6K2 primary structures. % Identity = 12.23% (relative to *E. histolytica* IP6K) and 15.01% (relative to human IP6K2). The mapping of *T. cruzi* colored protein structures was predicted by EMBL-EBI's Pictorial database of 3D structures in the Protein Data Bank (http://www.ebi.ac.uk/thornton-srv/databases/pdbsum).The coordinates of the highlighted structures in black boxes were estimated using *E. histolytica* IP6K's known structures as reference. The alignment was visualized using Jalview v2.11.1.5.

Afterwards, a well-elaborated substrate-bound structure of IP6K from *E. histolytica* was used to better imagine the relative amino acid positions and the structure of *T. cruzi* IP6K involving its interaction with IP_6. PyMol v2.5 was used to infer probable amino acids and chains involved in IP_6 phosphorylation. The *E. histolytica* IP6K/ATP/IP_6 complex was superimposed onto TcIP6K to elucidate the amino acids interacting with ATP and IP_6 in the substrate pocket of TcIP6K. In *E. histolytica*, the ATP is sandwiched between the N- and the C- lobes of its IP6K with its nucleotide binding not altering the protein conformation. Asp231 is found within its conserved DFA tripeptide, which coincides with Asp694 of the TcIP6K coordinating with two Mg^{2+} ions and establishing polar contacts with nucleotide phosphates. It should be noted that in this interaction, the γ-phosphate of ATP is flexible, contributing to low affinities of IP6Ks to this nucleotide (Figure 4).

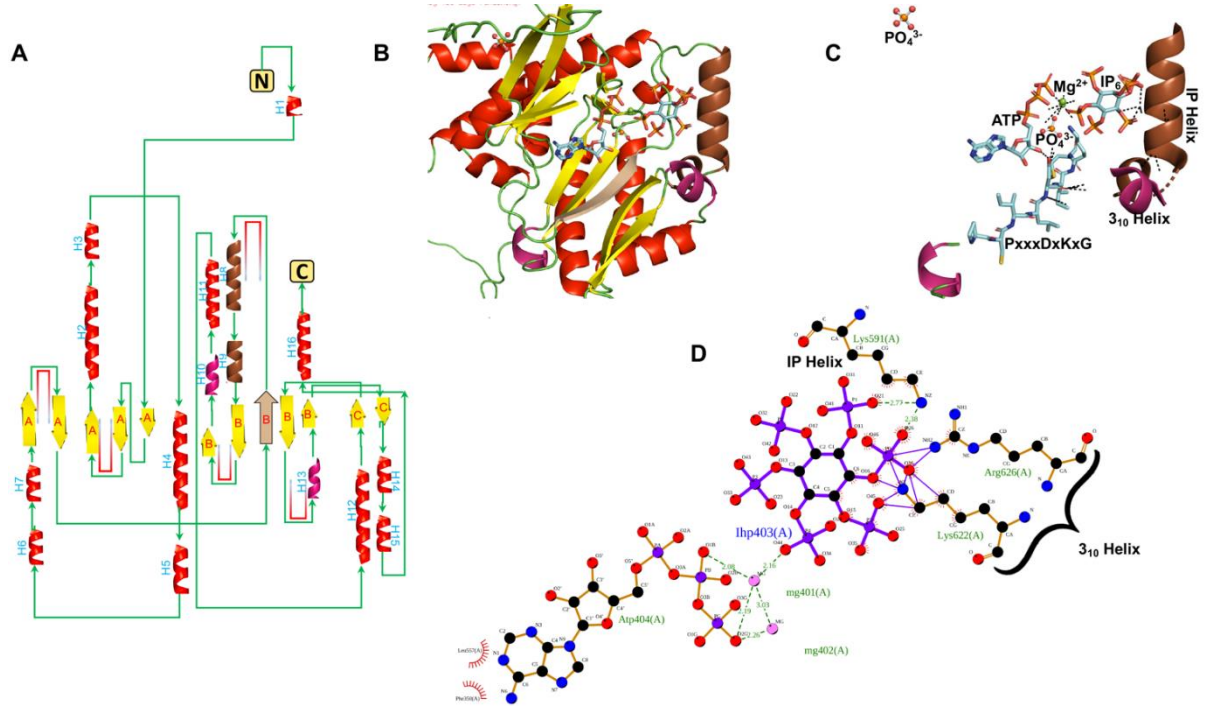

Figure 4. Secondary and tertiary structures predictions for IP6K from *T. cruzi* (CL Bener). A. *T. cruzi* IP6K topology as predicted by EMBL-EBI's Pictorial database of 3D structures in the Protein Data Bank (http://www.ebi.ac.uk/thornton-srv/databases/pdbsum). **B.** *T. cruzi* IP6K's secondary structure as predicted by AlphaFold2 (alphafold.ebi.ac.uk/) and superimposed on *E. histolytica* IP6K/ATP/IP_6 crystal structure from PDB (www.rcsb.org/structure/4O4F) for reference (Wang et al., 2014). The superimposition and substrate mapping were visualized by PyMolv2.5 (pymol.org/2/). *E. histolytica* IP6K secondary structure, except the ligands, was hidden to allow for the visualization of the *T. cruzi* IP6K. The strands are yellow, the helices are red and the loops are green. The Catalytic Motif strand and the IP helices are emphasized as light brown and dark brown respectively, while the 3_{10} helices are emphasized as pink. ATP and IP_6 are shown as licorice sticks (Light blue = Carbon, Dark Blue = Nitrogen, Red = Oxygen, Orange = Sulfur). Magnesium and Phosphorous ions are denoted as ball and sticks (Green balls = Magnesium ions, Orange balls = Phosphorous, Red balls = Oxygen, White sticks = Phosphorous-Oxygen Bonds). **C**. *T. cruzi* IP6K substrate pocket close up represented as licorice sticks bonded to interacting helices. Dotted black dashes represent polar contacts of interacting molecules. **D**. *T. cruzi* IP6K interacting with IP_6 in the substrate pocket visualized by EMBL-EBI's LigPlot+v2.2.7 (www.ebi.ac.uk/thornton-srv/software/LigPlus/download2.html) after exporting molecule B as a PDB file. The structure is represented as a ball and stick 2D figure (black balls = carbon, dark blue balls = nitrogen, red balls = oxygen, purple balls = phosphorous, pink balls = Mg^{2+} ions, orange sticks = non-IP_6 bonds, purple sticks = IP_6 bonds, green dotted lines = atom distances). The bottom left red-radiating structures represent amino acids involved in hydrophobic interactions.

In human, a highly-structured of 63-residues inositol-phosphate-binding domain creates four helices with larger constraints which both replace the IP helices in IP6Ks and also limits substrate activity to just IP_3 alone (Wang et al., 2014). The IPMK has been shown to have lost the 3_{10} helix but whose substrate pocket remains large still allowing its promiscuity at the 3-, 4- and 6- positions. This promiscuity is a shared characteristic of ITPK1 which has a 1-, 5- and 6- phosphorylation activities of the inositol phosphates (Wang et al., 2014). Mammalian IP6Ks have also been shown to phosphorylate IP_5 to PP-IP_4 (Choi et al., 2007; Fridy et al., 2007; Shears et al., 2017). Within the substrate pockets of IPMK and ITPK1, the plane of inositol rings in all of the alternate substrates are

hypothesized to occupy a similar spatial orientation making it possible for the different substrates to interact with common regions of kinase contacts (Yang et al., 2000; Shears, 2004; Miller et al., 2005; Holmes et al., 2006; Chamberlain et al., 2007; Endo-Streeter et al., 2012).

It was possible to determine that the ATP in a supposed TcIP6K/ATP/IP6 complex is anchored by Pro564, Cys565, Ile566, Leu567, Asp568, Ile569, Lys570, Met571 and Gly572 around its PxxxDxKxG catalytic motif. The N^1 and N^6 atoms of Adenine have hydrogen bonds to surrounding amino acid residues anchoring the ATP in a hydrophobic pocket around Leu557 and Phe350 while its ribose group is confined by Van der Waals forces of attraction. Similar to *E. histolytica* IP6K/ATP/IP_6 complex, the IP_6 in TcIP6K/ATP/IP_6 complex lies in a shallow depression on its "open clamshell"-like jaws. This makes it possible that it interacts with amino acids Lys591 from the IP Helices, and Arg626 and Lys622 from the first 3_{10} helix, among others in the surrounding IP helix and 3_{10} helix. Like in *E. histolytica* IP6K, the γ-phosphate of ATP within the TcIP6K/ATP/IP6 crystal complex, this spatial arrangement supports phosphorylation of the 2-OH group.

In *E. histolytica*, the IP helix and the 3_{10} helix are not connected but are found in close proximities to warrant the metaphorical "hinge" to its clamshell shape (Wang et al., 2014). It is also worth noting that both the IP helix and 3_{10} helix interacting with IP_6 in TcIP6K are estimated from a known position of these helices in *E. histolytica* IP6K – just after the PxxxDxKxG catalytic motif - within amino acids 581-601 and 621-627 respectively. IP_6 plane in *E. histolytica* as in *T. cruzi* runs parallel to 3_{10} helix's contour thus facilitating the 4- and the 6-phosphates to interact with Arg152 and Tyr153, stabilized by cation-pi interactions between these two amino acids (Wang et al., 2014). This interaction is facilitated by the architecture of the 3_{10} helix implying the same interactions for amino acids Ser621 and Lys622 of TcIP6K.

Understanding the structure and evolution of TcIP6K makes it possible for this kinase to be explored as a viable drug target, which can also facilitate substrate-inhibitor interactions. Indeed, mutagenic analyses of Lys243, Cys257Glu, Lys274Ala and Tyr275Ala in human IP6K2 have shown that their disruptions affect interactions with the 6-phosphate IP_6. This is functionally significant since the mutated IP6K decreased its kinase activity 600-, 14-, 55- and 8-fold respectively for each of the amino acids stated above (Wang et al., 2014). Finally, it should be noted that this data extrapolation can further be supported and verified by crystallization experiments to definitively determine the interaction of TcIP6K with its substrates.

4.2 Disruption of IP6K alleles was efficiently accomplished using CRISPR-Cas9 system

To further investigate the possible functions of IP6K (and possible functions related to DNA repair, as proposed in the original project), we performed a loss-of-function approach using the CRISPR/Cas9 system. The first round of transfections ('sgRNA' and donor DNA) was done using a

T. cruzi lineage expressing T7/Cas9 cassette as a background (generated in collaboration with Dr. Simone Calderano – Butantan Institute). A gene disruption approach was used, whereby the 'sgRNA' was designed to guide Cas9 to cut the DNA, not at the beginning and end of the gene but at its intergenic regions.

T. cruzi CL Brener strain is a diploid organism with naturally occurring hybrid of both Esmeraldo-Like (EL) and Non-Esmeraldo-Like (NEL) haplotypes (El-Sayed, 2005), being classified as TcIV, according to the discrete typing units (DTUs) (Zingales et al., 2012). Thus, we designed 'sgRNA' toward sites that had consensus regions between the two IP6K alleles [TcCLB.504213.90 (EL) and TcCLB.506985.60 (NEL)]. A brief search at TritrypDB shows that IP6K alleles occur at chromosome 11. Despite these alleles being homologous, their UTRs have slight differences, which led to the adoption of the gene disruption approach (Figure 5).

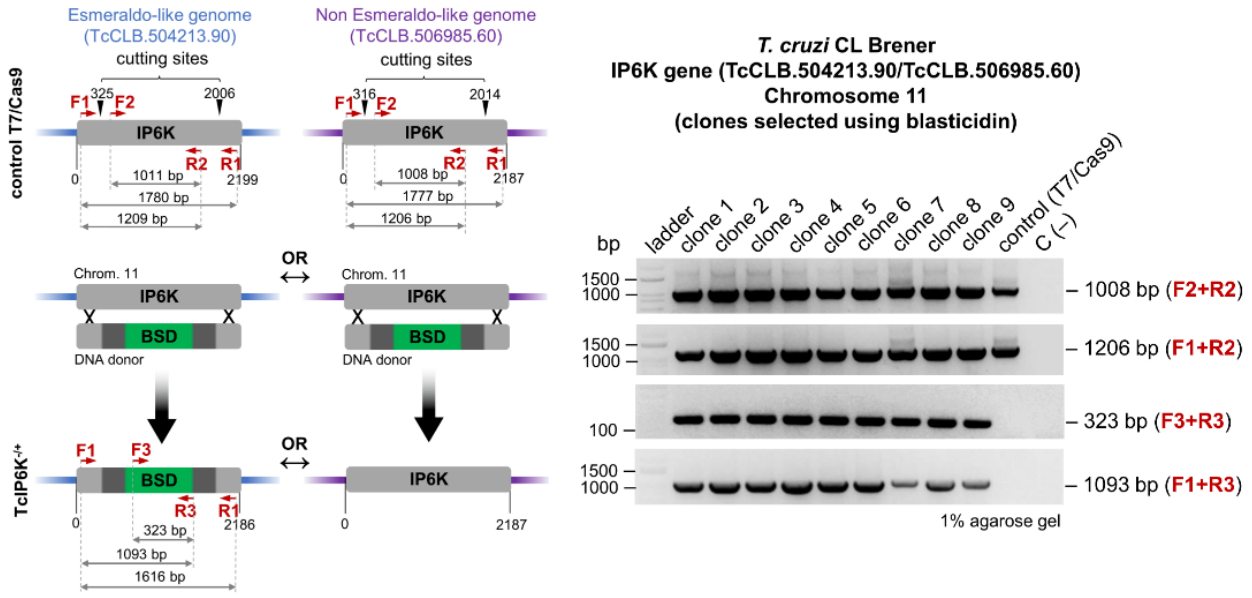

Figure 5. CRISPR/Cas9 system is an efficient approach to disrupt IP6K alleles. Left: scheme showing the gene disruption strategy used and the primers position used in the following PCRs. **Right:** PCR results confirming the presence of donor DNA (containing a blasticidin-resistance gene) and target DNA (IP6K gene) both at the correct loci in all the nine clones selected. Cells expressing T7/Cas9 were used as a background to perform the CRISPR/Cas9 editing.

The 1° round of transfection was done using a donor DNA containing blasticidin-resistance gene. The PCR results of the nine clones selected confirmed the presence of the blasticidin-resistance gene inserted at the correct loci. However, our results also showed the other copy of IP6K in its correct locus, evidencing a single-null (IP6K$^{-/+}$) lineage.

The inability to perform a complete knockout of this gene in one round of transfection seems to reflect on the hypothesis that perhaps the IP6K is an essential gene. However, we persist to try disrupting the remaining IP6K copy performing one more transfection round.

The 2° round of transfection was done to achieve a double-null (IP6K$^{-/-}$) lineage. This was done using a donor DNA containing a puromycin-resistance gene and one of the previous selected clones (clone 2) from the first round of transfection as background (Figure 6).

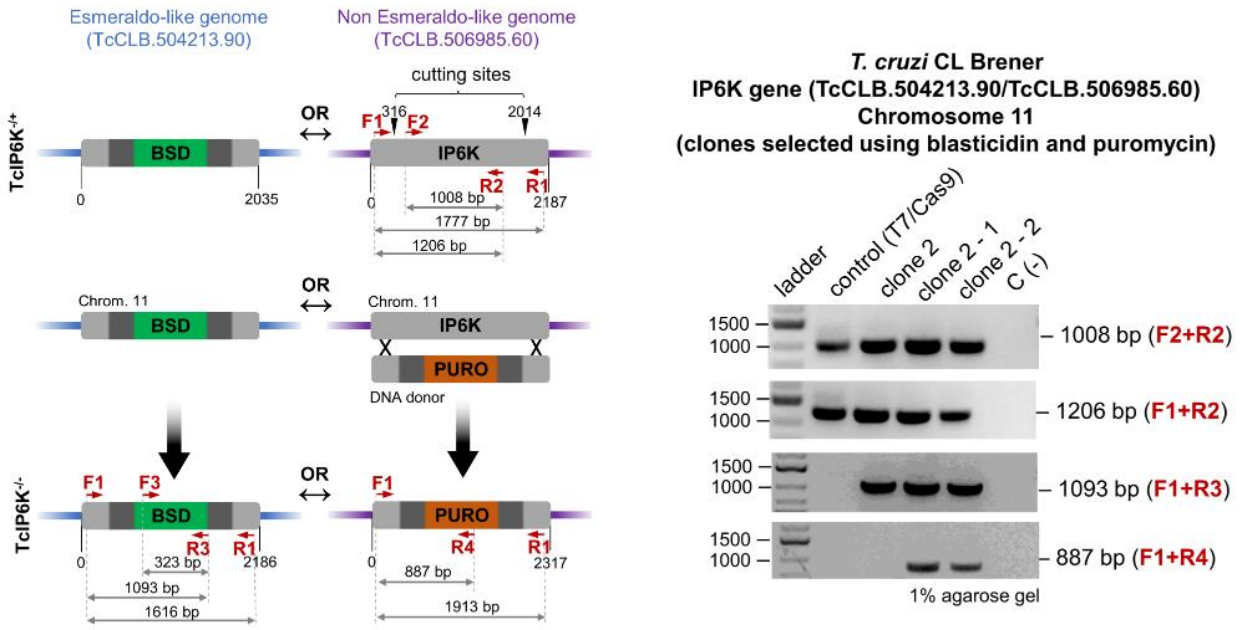

Figure 6. Second round of transfection using IP6K$^{-/+}$ lineage as a background to disrupt the remaining IP6K allele. Left: scheme showing the KO strategy used to confirm the efficacy of IP6K knockout using a standard PCR. **Right**: PCR results confirm the presence of both donor DNAs (blasticidin and puromycin) at the correct loci in all the selected clones. The IP6K was also detected at the correct loci in this analysis probably because we were unable to select clones after the second round of transfection, since the obtained population was unable to proliferate. Clone 2 from the first round of transfection was used as a background for the second round of transfection.

PCR results of the second round of transfection revealed the presence of double-null (IP6K$^{-/-}$) lineages, presenting the donors DNA containing puromycin- and blasticidin-resistance genes inserted at the correct loci. However, we also detected the IP6K gene inserted in their original loci (Figure 6, primers F2+R2 and F1+R2). This happened probably because we were unable to select clones after the second round of transfection, since the obtained population was unable to proliferate (see results onward). Thus, single-null lineages (or even their DNA) could be present during DNA extraction, masking the results. Of note, the inability to proliferate point that IP6K is probably essential for *T. cruzi* CL Brener.

4.3 Disruption of IP6K impairs *T. cruzi* epimastigotes proliferation

To check the proliferation ability of the *T. cruzi* lineages generated, we chose one IP6K clone from previously selected and performed growth curves together with WT and T7/Cas9 lineages (Figure 7). As observed after the second round of transfection, the generated polyclonal lineage

(TcIP6K$^{-/-}$) was apparently unable to proliferate. To confirm this suspicion and verify the proliferation capacity of the generated *T. cruzi* lineages, we performed growth curves (Figure 7A). The wild-type (WT) and T7/Cas9 *T. cruzi* lineages did not show significant differences (green and gray lines) (Figure 7A). Thus, for the onward assays, we used only T7/Cas9 as our parental control. Moreover, as expected, the double-null lineage (IP6K$^{-/-}$) did not show a progressive growth, which evidences its inability in proliferating (red line). Also, the single-null lineage (IP6K$^{-/+}$) (blue line) showed a slight growth delay relative to the control (T7/Cas9). This finding suggests that loss of the IP6K gene significantly contributed towards lack of growth (in case of IP6K$^{-/-}$) or delay (in case of IP6K$^{-/+}$), suggesting important functions for IP6K.

To confirm the downregulation of IP6K in the single null lineage (IP6K$^{-/+}$) relative to the control (T7/Cas9), we carried out RT-qPCR using GAPDH as endogenous control to normalize IP6K expression (Figure 7B). As expected, the expression of IP6K significantly dropped by half (Figure 7B). Figure 7C show the quality of the total RNA used in our RT-qPCR assays. Figure 7D shows violin plots of the Ct values (for GAPDH and IP6K) obtained from quadruplicated assays. It is worth to mentioning that we were unable to extract total RNA from the double null (IP6K$^{-/-}$) lineage, as this population showed serious impairment in its proliferative capacity, as observed by the growth curves (Figure 7A – red line). However, we were able to use this lineage (IP6K$^{-/-}$) to perform some other assays, as we will see onward.

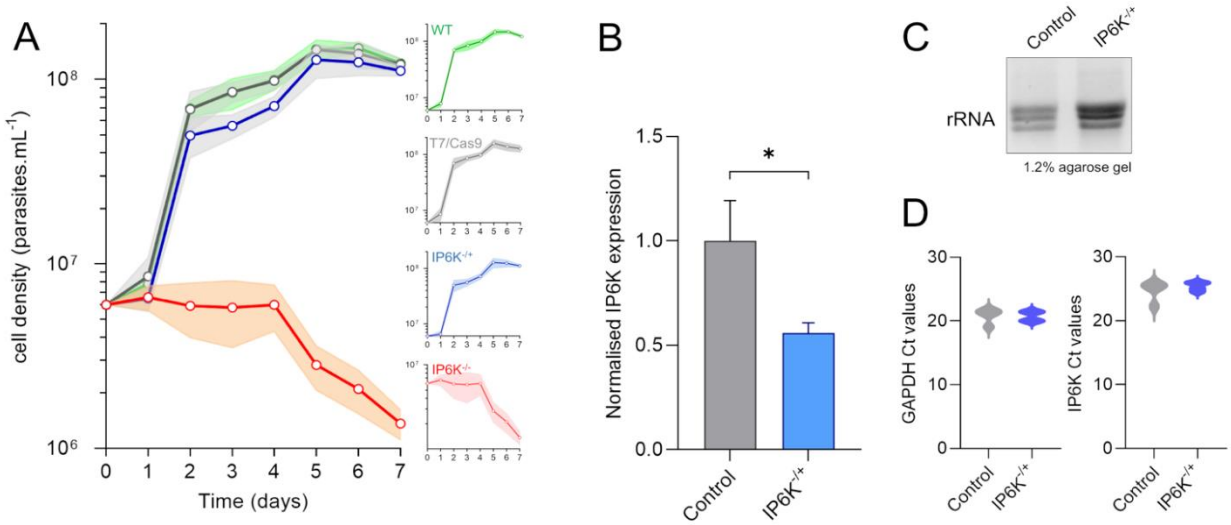

Figure 7. Growth curves and RT-qPCR analyzes confirm the disruption of IP6K in *T. cruzi* (CL Brener). **A**. All growth curves (WT, T7/Cas9, IP6K$^{-/+}$, and IP6K$^{-/-}$) started from 6.10^6 parasites.mL^{-1}. Using these curves, it was possible to estimate de doubling-time for each lineage analyzed (8 h for WT and T7/Cas9, and 8.2 h for IP6K$^{-/+}$). This estimative was done taking the values at exponential phase and using Doubling Time software version 1.0.10 (http://www.doubling-time.com). Shaded area in each curve represents the standard error of the mean (± SEM) from three independent experiments. **B.** RT-qPCR results showing the normalized expression of IP6K. **C.** Total RNA (1 µg) pattern used in RT-qPCR assays. The three bands evidenced in 1.2% agarose gel represents the different subunits of ribosomal RNA (rRNA). **D**. Ct values for GAPDH and IP6K, obtained from quadruplicated assays.

The most interesting finding, as expected, is that the double-null (IP6K$^{-/-}$) lineage did not show a progressive growth, which evidences its inability in proliferating (red line). Also, the single-null (IP6K$^{-/+}$) lineage showed a slight growth delay relative to the T7/Cas9 (blue line). This finding suggests that loss of the IP6K gene significantly contributed towards lack of growth (in case of IP6K$^{-/-}$) or delay (in case IP6K$^{-/+}$), suggesting important cellular functions for IP6K. Recently, a study characterizing the inositol pyrophosphates biosynthetic pathway in *T. cruzi* (Y strain) suggested that IP6K single null depletion impair cell morphology and growth (Mantilla et al., 2021a). Similarly, another study performed in *Crypotococcus neoformans* revealed that Kcs1 KO (Kcs1 is the IP6K ortholog in Fungi) showed decreased growth rates compared to wild-type cells (Lev et al., 2015). This research postulated that this phenotype was attributed to defects in biosynthetic pathways of key macromolecules like nucleotides and fatty acids that depend on mitochondrial enzymes. In other words, IP6K is probably an essential gene. However, further assays, such as conditional IP6K knockout, must be done to support this hypothesis.

From the growth curves it was also possible to estimate the doubling time (dt) for these lineages (except for the double nulls), which was found to be around 8 h (for WT and T7/Cas9), with the IP6K$^{-/+}$ having a slightly longer dt (8.5 h). Of note, the dt for *T. cruzi* CL Brener (WT) lineages disagrees with an older study, which pointed the doubling time for epimastigotes of *T. cruzi* CL Brener as ~58 h (Zingales et al., 1997), but it is close to more recent studies (Alves et al., 2018; Resende et al., 2020). A possible explanation for this discrepancy is that we do not use antimycotic in our LIT medium, which could delay the growth of *T. cruzi*. However, further studies are needed to collect more evidence to support this hypothesis.

Given the fact that the IP6K KO lineages showed slow growth rate (or no growth as showed by IP6K$^{-/-}$), it was important to explore their phenotypes further, such as possible morphological alterations and possible cell cycle arrest.

4.4 IP6K is located predominantly in the cytoplasm of *T. cruzi* (CL Brener)

To investigate the subcellular localization of IP6K, we used the M9 lineages (negative ribozyme control in an ongoing research project) in IFA. Use of M9 but not Overexpression lineages was justified through preliminary confirmation by PCR that the M9 construct was added to the 3' UTR of IP6K, including the HA tag, whose expression could not be followed in the overexpression lineages, i.e., the use of HA to tag IP6K could not be established via Western Blot, possibly because the epitope that the anti-HA antibody recognize requires is structural, which is destroyed by denaturing conditions of SDS-PAGE. In a recent study, Hortua-Triana et. al., (2018) established detection by both immunofluorescence and western blot of weakly expressed *T. gondii* calcium-related genes tagged with HA. We tried to do the same here.

We tagged both TcIP6K alleles (TcCLB.504213.90 – Esmeraldo-Like and TcCLB.506985.60 – Non-Esmeraldo-Like). TcIP6K was shown to be localized throughout the entire cytoplasm (Figure 8), which support that idea that PP-IPs (in this case IP_7) may be involved in a high number of cellular pro

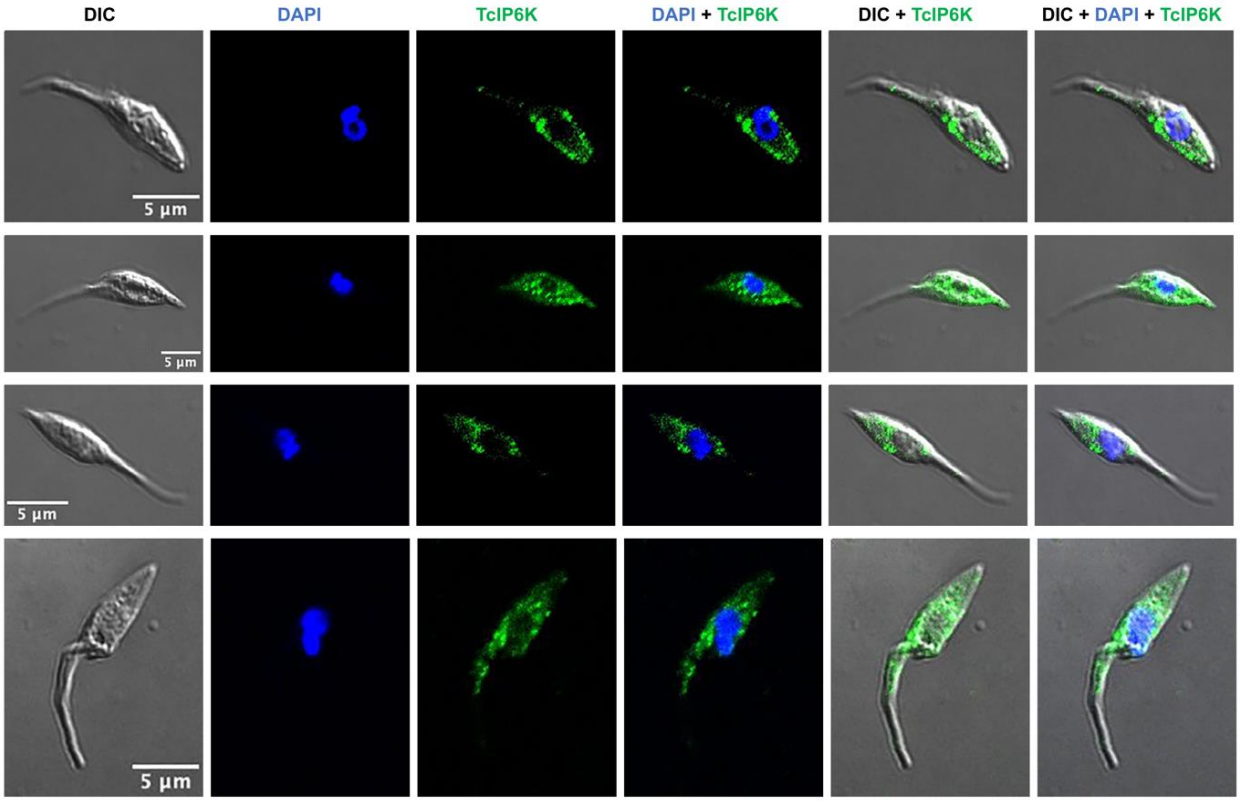

Figure 8. Subcellular localization of IP6K in *T. cruzi* (CL Brener). The generated lineage (M9 - negative ribozyme control containing 3xHA tag) were used to acquire representative images [DIC, DAPI, TcIP6K and merged images, (DAPI+TcIP6K, DIC+TcIP6K and DIC+DAPI+TcIP6K)].

TrypTag (http://tryptag.org/?pageType=landing), an online-based service project that aims to determine the subcellular localization (by microscopy) of every trypanosome protein (Dean et al., 2016), was able to tag *T. brucei* IP6K (Tb927.7.4400) using mNeonGreen (Shaner et al., 2013). The service, wherever possible, determines the localization of the protein of interest by tagging at both the N and C terminus. They use long PCR primers (Dean et al., 2015) to make the tagging amplicons and then transfect the trypanosomes with the PCR products in 96-well electroporation plates (Dyer et al., 2016). The results of this service show that Tb927.7.4400 can be tagged at the C and N termini in one attempt whence it was shown that Tb927.7.4400 occurred in 75% of the general cytoplasm weakly distributed as such: cytoplasm (25%), flagellar cytoplasm (25%) and in nuclear lumen (25%) (http://tryptag.org/?query=Tb927.7.4400). These patterns are somewhat similar to those presented by *T. cruzi*, alluding to similar functions of IP_7 in kinetoplastids.

4.5 Disruption of IP6K alters cell morphology and FKN patterns of *T. cruzi*

Analyses using SEM (Scanning Electron Microscopy) and TEM (Transmission Electron Microscopy) was performed in collaboration with Dr. Maria Cristina M. Motta (Federal University of Rio de Janeiro – UFRJ) to observe deeper the morphological alterations in the IP6K KO lineages generated (IP6K$^{-/+}$ and IP6K$^{-/-}$). There was evidence of altered cellular morphology and cell organelles. Diverging from the typical epimastigote forms, the single-null lineages (IP6K$^{-/+}$) showed rounding of the cell body, especially at the anterior region next to the flagellum (arrows on Figure 9A). These lineages also presented shortening and wrinkling of the cell body. The IP6K double-nulls (IP6K$^{-/-}$) showed further shortening, rounding and wrinkling of the cell body. They also present aberrant cell features such as multiple flagella pointing to phenotypes impediment to cell division.

The TEM further revealed changes in organelle composition of the IP6K lineages (Figure 9B). In both single-nulls and the double-nulls, there is an increase in the number of glycosomes (g) and enlargement of mitochondrial branches (*). Also, there are several cells showing two basal bodies close together (arrows on Figure 9B) and kinetoplast with duplicated kDNA which may be indicative of arrest of cell division, which coincides with the phenotypes observed by SEM. The observed increase in the number of glycosomes was especially interesting, pointing to changes in cell metabolism of the IP6K$^{-/+}$ lineages. This phenomenon presents excellent opportunities to further explore the effect of IP6K loss in different metabolic pathways during *T. cruzi* differentiation.

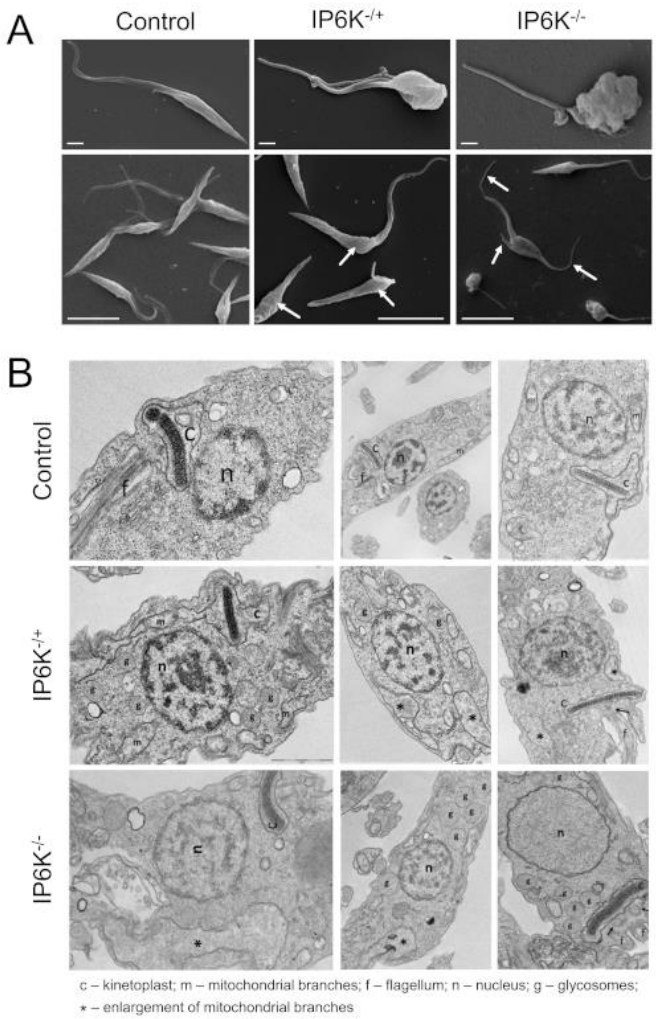

Figure 9. Disruption of IP6K alters cell morphology in *T. cruzi* CL Brener. The generated lineages (Control, IP6K$^{-/-}$, and IP6K$^{-/+}$) were analyzed using (**A**) Scanning Electron Microscopy (SEM), and (**B**) Tunnel Electron Microscopy (TEM). C = kinetoplast, m = mitochondrial branches, f = flagellum, n = nuclei, g = glycosomes, * = enlargement of mitochondrial branches.

The FKN (flagellum, kinetoplast, and nucleus) patterns are often used to verify alterations in cell morphology and cell cycle phases in trypanosomatids (Marin et al., 2018), since through these patterns is possible to infer cell cycle phases distribution: G1/early S (1F1K1N), late S (2F1K1N), G2/mitosis (2F2K1N), and cytokinesis (2F2K2N), and verify abnormal/aberrant cells (any FKN pattern other than those previously mentioned). Using this approach, we analyzed the *T. cruzi* lineages generated. We found that the single-null lineage (IP6K$^{-/+}$) showed a higher number of cells with the 1F1K1N pattern relative to the control, which suggests a possible cell cycle arrest (Figure 10).

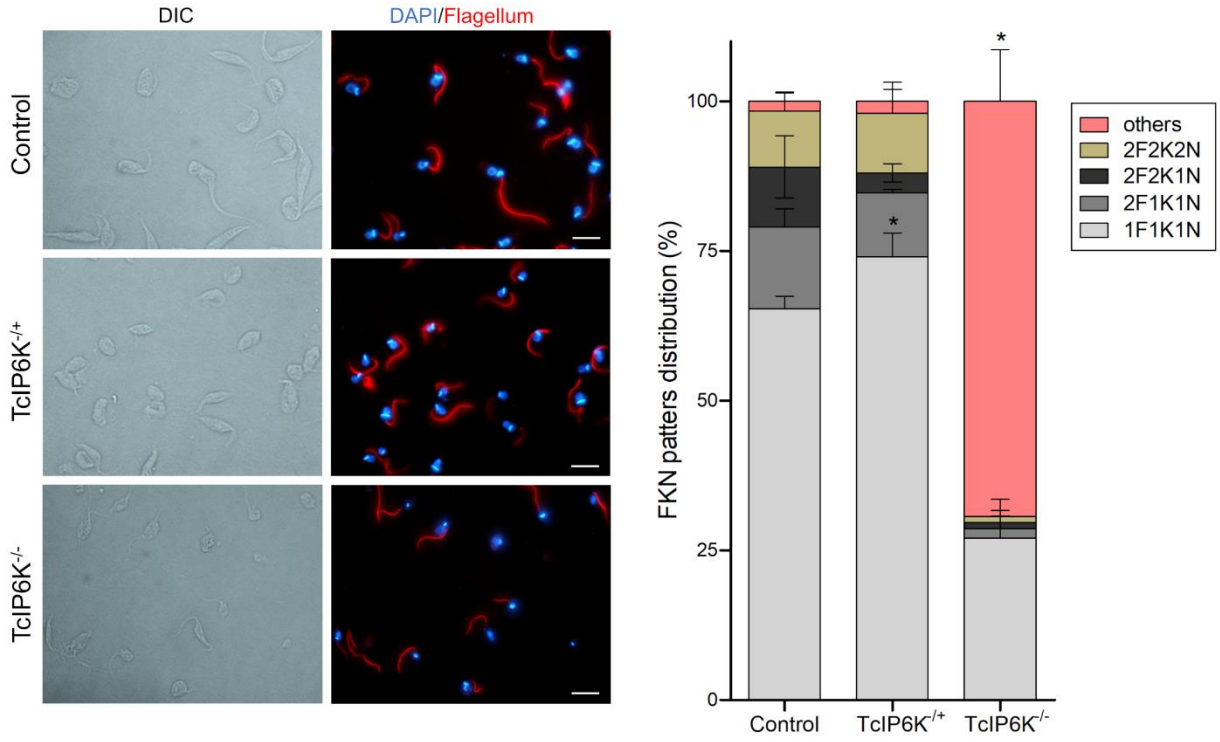

Figure 10. Disruption of IP6K alters FNK patterns. Left: representative images [DIC and merged (DAPI+flagellum)] evidenced the different patterns found in the three *T. cruzi* lineages analyzed. Right: Quantification of the different FKN patterns in each *T. cruzi* lineage analyzed. The data represent the average of three independent experiments and the error bars represent the standard deviation from more than 300 cells analyzed per sample. (*) The difference observed was statistically significant using Student's t-test ($p<0.01$).

Furthermore, the double-nulls (IP6K$^{-/-}$) showed a high number of aberrant cells (others) evidencing that the FKN pattern in the absence of IP6K is totally compromised (Figure 10). Also, some cells of this lineage presented curious alterations, such as multiple flagellum and non-fusiform morphology corroborating the results elucidated by the SEM (Figure 9A). This could be due to

affected pathways involving cell membrane, organelle division and segregation. Although cell cycle progression is a tightly regulated process, the PP-IPs levels exhibit a dynamic behavior throughout the cell cycle phases (Barker et al., 2004).

PP-IPs have been found to be high during the G1 phase, drop during the S phase and then increase later in the cell cycle stages. These fluctuations are in tandem with different events occurring during cell proliferation such as gene transcription, cytoskeleton formation, nuclear mRNA export and chromatin remodeling, among others (Shah et al., 2017). Interference with cellular IP_7 could therefore interfere with normal *T. cruzi* metabolic functions during cell cycle, leading to formation of aberrant lineages, as observed.

4.6 Disruption of a single IP6K allele arrests *T. cruzi* cells in G0/G1 phase

To investigate further the possible cell cycle arrest in the single-null ($IP6K^{-/+}$) lineage, we performed a DNA content analysis using flow cytometry. Also, we included in this analysis the double-null lineage ($IP6K^{-/-}$) (Figure 11).

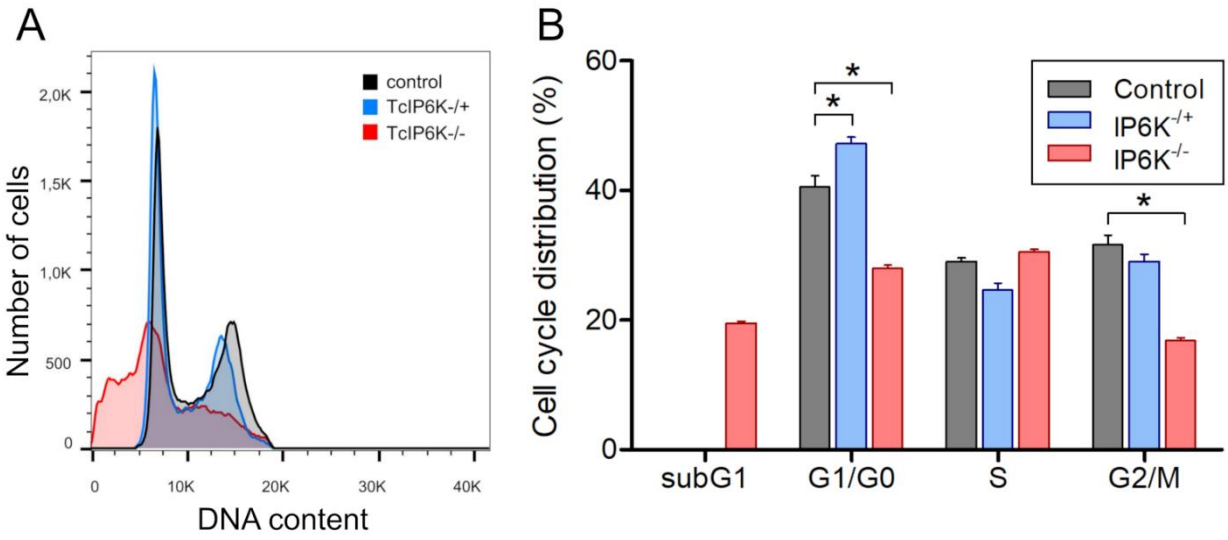

Figure 11. Disruption of a single IP6K allele leads to G0/G1 cell cycle arrest. A. Histograms overlay of the lineages analyzed. **B.** Quantification of the cell cycle phases inferred using FlowJo software. These assays were carried out in biological triplicate, and at least 50,000 cells (n=50,000) were analyzed per sample. Errors bars indicate SD. The difference observed was statistically significant using Student's t-test ($p<0.01$).

Our findings suggest that the single-null ($IP6K^{-/+}$) lineage presented a slight cell cycle arrest at G0/G1 phase relative to control, while the double-null ($IP6K^{-/-}$) presented a pronounced sub-G1 DNA content, suggesting the presence of cell death (DNA fragmentation). The cell cycle arrest at G0/G1 phase could be generated either by DNA damage or increased G0 state (quiescent) cells. As previously mentioned, PP-IPS levels were noticed to fluctuate during the cell cycle progression (Barker et al., 2004), which could justify this slight G0-state arrest. In other words, the cells accumulation at G1 phase/G0-state can be reflecting the PP-IPs reduction during the eventual

termination of the cell cycle progress. Although preliminary, these data suggest the PP-IPs could play an important role during the transition of the cell cycle phases in *T. cruzi*.

4.7 Disruption of a single IP6K allele slight alters the cell cycle phases length in *T. cruzi*

To investigate further the cell cycles phases, we applied calculations based on specific parameters to estimate the cell cycle phases duration in the IP6K$^{-/+}$ lineage relative to control (Figure 12). More details about this approach can be found in other studies carried out by our group (da Silva et al., 2013, 2017, 2020).

As expected, there are slight changes in the cell cycle lengths when comparing the control and single-null (IP6K$^{-/+}$) lineage (Figure 12). This data corroborates the previous DNA content analyzes (Figure 11) and support the hypothesis that perhaps IP_7 is needed for a successful progression of the cell cycle phases. The low levels of this metabolite perhaps impair the cell cycle commitment, leading part of the population to remain quiescent (G0-state).

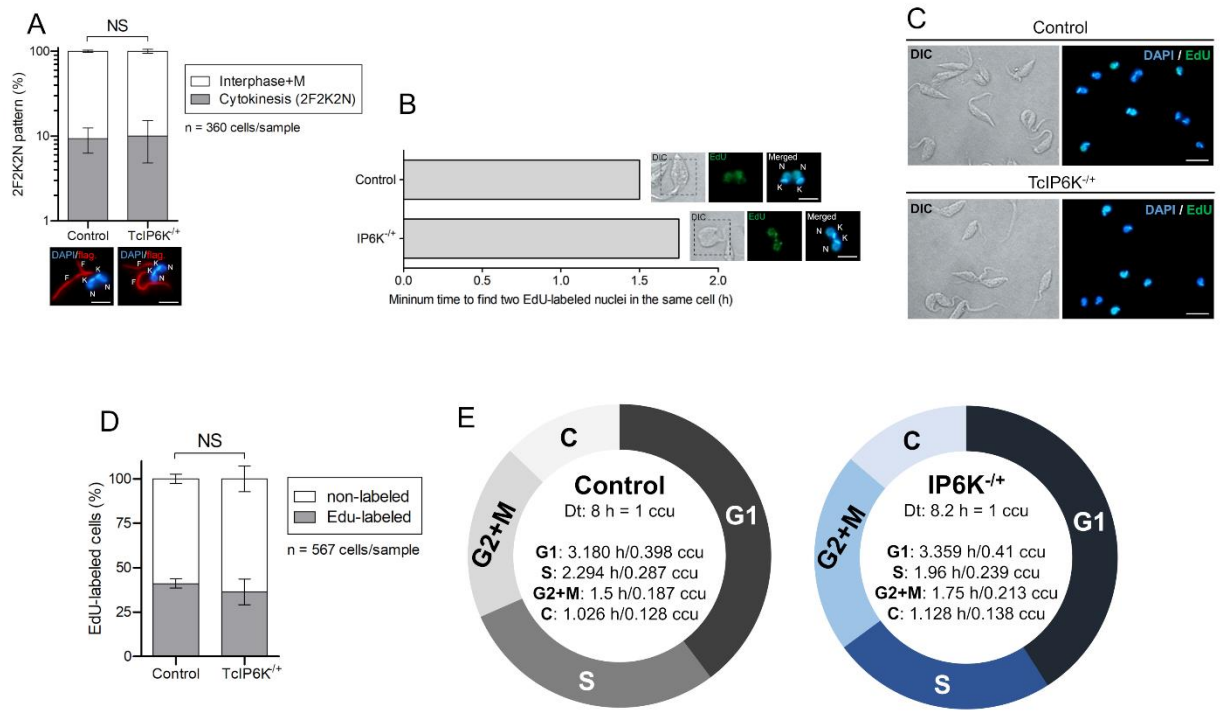

Figure 12. Single null (IP6K$^{-/+}$) lineage presents slight alterations in the cell cycle phases duration. A. Quantification of cells in the cytokinesis phase (2F2K2N) determined by the FKN patterns analysis. **B.** The minimum time taken for the 2K2N pattern to appear in one cell through EdU-labeled. **C, D.** Proportion of cells able to take up EdU after 1 h. **E.** Estimation of the cell cycle phases duration made using the previous parameters and the CeCyD software (cecyd.vital.butantan.gov.br/) (da Silva et al., 2020). The doubling time for the two lineages were estimated by taking the values at exponential phase and using Doubling Time software (http://www.doubling-time.com).

As previously mentioned, recent studies reported that the fluctuation of PP-IPs during the cell cycle progression could be signaling important pathways involved during the transition phases in which PP-IPs modify other molecules through binding or phosphorylation post-transcriptionally (Barker et al., 2004; Shah et al., 2017). Anyway, more studies are needed to tease out these possible important physiological functions played by PP-IPs.

4.8 Disruption of a single IP6K allele leads *T. cruzi* to quiescence without DNA damage

The cellular decision to progress in the cell cycle is mediated by a specific cell cycle control machinery, which responds to various internal and external signals (Pack et al., 2019). Moreover, distinct mechanisms act in concert to mediate cell cycle arrest, normally due to DNA damage (Toettcher et al, 2009). To investigate the presence of DNA damage into the generated lineages, we carried out IFA using α-γH2A antibody, a DNA damage biomarker (Figure 13). Of note, phleomycin causes generalized DNA damage *in vitro* (Sleigh, 1976), and due to that, it was used as a positive control (da Silveira et al., 2012) (Figure 13).

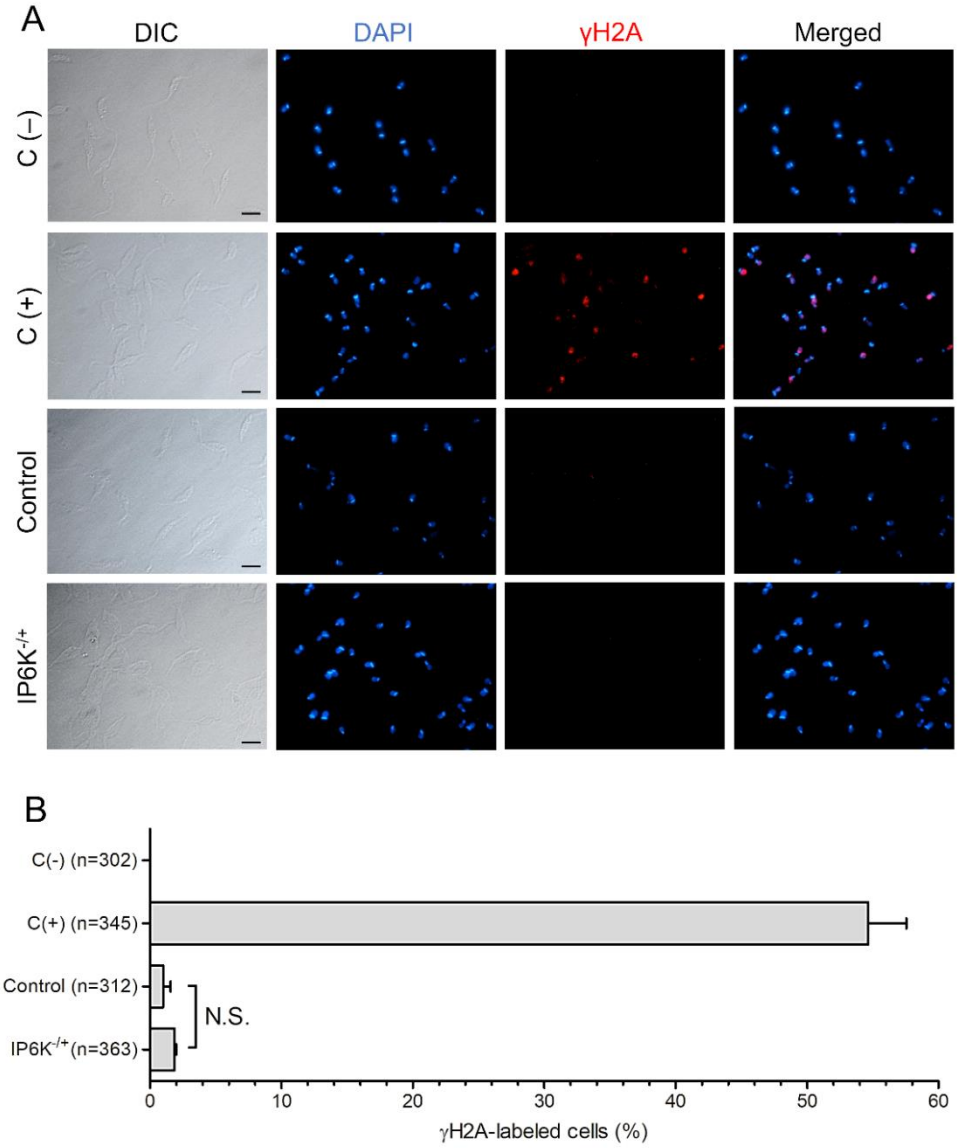

Figure 13. Disruption of a single IP6K allele does not cause DNA damage in *T. cruzi*. A. Immunofluorescence assay (IFA) evidencing the absence of endogenous γH2A foci in the control and IP6K$^{-/+}$ lineage. The negative control [C(-)] was made replacing α-γH2A primary antibody by PBS. The positive control was carried out pre-treating the control sample with 200 µg.mL^{-1} phleomycin for 1 h. DAPI was used to stain organelles containing DNA: nucleus and kinetoplast. Bars = 5 µm. **B**. Quantification of the cells presenting γH2A foci. The error bars represent the standard deviation (SD) from an assay performed in triplicate (n = 300). N.S. = non-significant according to Student's t-test (p>0.05).

Surprisingly, we found no DNA damage in the analyzed lineages (Figure 13). This finding therefore led us into testing the second reason that could explain the G1/G0 cell cycle arrest observed in our results: increased number of quiescent cells. Quiescence is a state of reversible proliferative arrest in which cells are not committed to cell division but still retain the capacity to reenter the cell cycle upon receiving an appropriate stimulus (Marescal and Cheeseman, 2020). Based on this definition, we developed a pioneering method to quantify cells not committed to the cell cycle (quiescent – dormant cells) considering on the cell cycle phases length previously estimated (Figure 12) and DNA replication monitoring by EdU. We named this essay as EdU-negative selection (Figure 14).

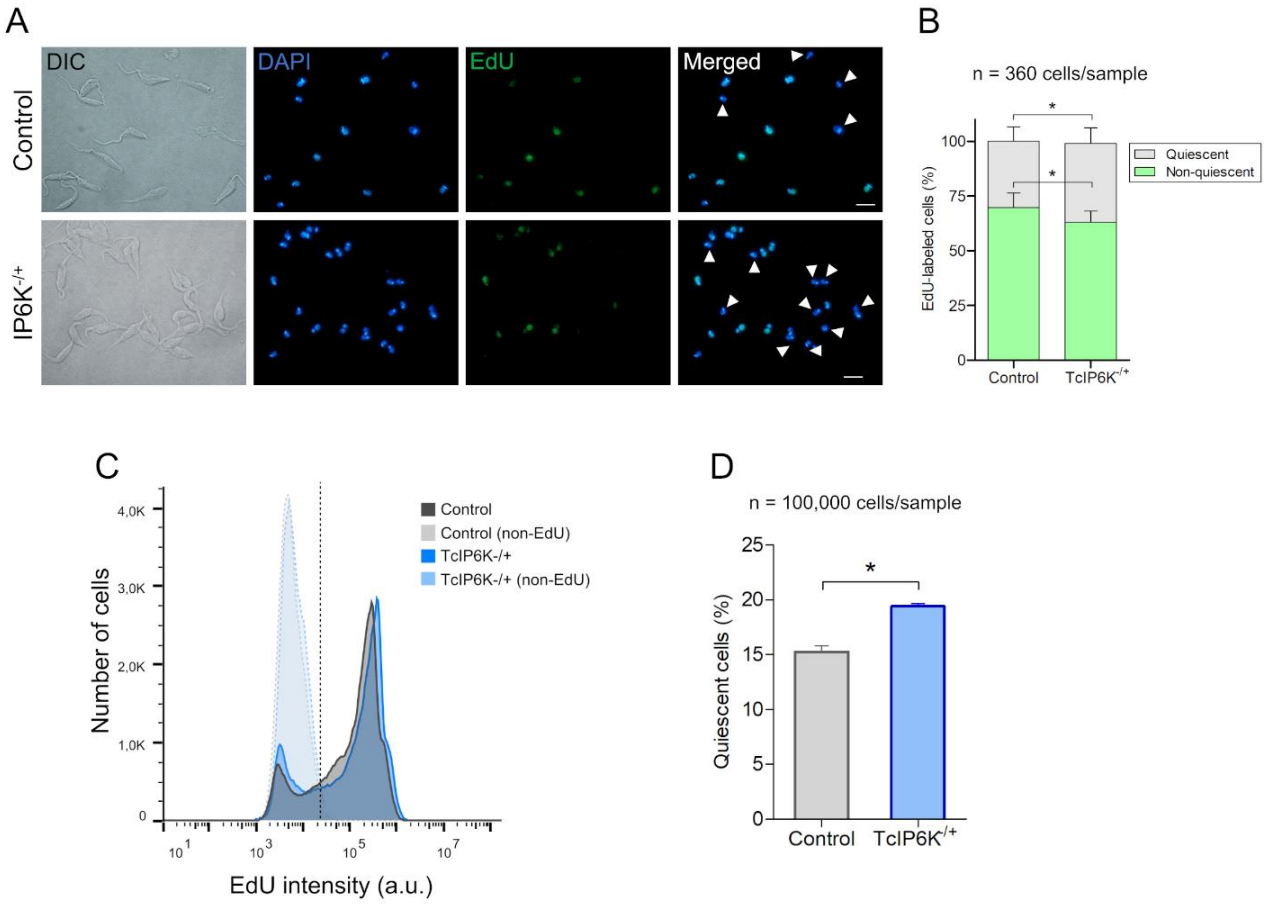

Figure 14. Disruption of a single IP6K allele increases the number of quiescent *T. cruzi* cells. A. DNA replication monitoring (using EdU incorporation for 8 h) evidencing that IP6K$^{-/+}$ lineage presents fewer EdU-labeled cells (white arrows). DAPI was used to stain organelles containing DNA: nucleus and kinetoplast. Bars = 5 µm. **B**. Quantification of the EdU-labeled and non-labeled cells. The error bars represent the standard deviation (SD) from an assay performed in triplicate (n = 360/sample). * = p< 0.05 using Student's t-test. **C**. Overlapped histograms of the control (grey) and IP6K$^{-/+}$ (blue) lineages analyzed by flow cytometry. The same lineages were cultivated in the absence of EdU, being used as non-labeled control [control (light gray) and IP6K$^{-/+}$ (light blue)]. 100,000 cells were analyzed per sample in an assay performed in triplicate. **D**. Measurement of the EdU-labeled and non-labeled cells presented in C. The measurement was made using the FlowJo software. The error bars represent the standard deviation (SD) from an assay performed in triplicate (n = 100,000/sample). * = p< 0.05 using Student's t-test.

Our findings, both by IFA (Figure 14A-B) and by flow cytometry (Figure 14C-D), suggest that the IP6K disruption contributed to the increased number of quiescent cells in *T. cruzi* (CL Brener) as they did not have pre-existing DNA damage. Through IFA, we identified fewer Edu-labeled cells in IP6K$^{-/+}$ lineage, consequently, more quiescent cells (Figure 14B). By flow cytometry, the same lineage presented a slightly higher Edu-non-labeled peak (blue peak on the left side), which represents quiescent cells (Figure 14C).

Recently, a research group demonstrated that *T. cruzi* amastigotes can reach a quiescent state called dormancy, responsible for evading the action of antitrypanosomatid compounds (Sánchez-Valdéz et al., 2018). Our findings suggests that the increased quiescent cells observed in our analyzes could be a type of dormancy for epimastigote *T. cruzi* forms. However, we still do not have enough data to correlate dormancy between *T. cruzi* amastigotes and epimastigotes. Another possibility is that the quiescent cells observed could be metacyclic (infective) forms of *T. cruzi*. In other words, the depletion of a single IP6K allele could trigger a response that causes *T. cruzi* to become more infective. To investigate this hypothesis, we carried out and infective assay to measure the multiplication capacity inside the cell host.

4.9 *T. cruzi* IP6K$^{-/+}$ lineage presents increased multiplicative capacity within the host-cell

To investigate the multiplicative capacity of single-null (IP6K$^{-/+}$) lineage, we established a pilot assay using Vero and HeLa cells. First, the epimastigotes from IP6K$^{-/+}$ lineage were differentiated into metacyclics trypomastigotes forms, which were used to infect Vero cells. After transforming into amastigotes and multiplying inside Vero cells, the amastigotes transform into TCTs, and hatch from the cell. The released TCTs were then labelled using CFSE and used to infect HeLa Cells (MOI 50:1). After 72h, the HeLa cells were washed, trypsinized and analysed by flow cytometry (Figure 15A). A portion of the cells were collected and labeled with Giemsa stain, where it is possible to verify that, apparently, a higher number of amastigotes is found inside the HeLa cells infected with the IP6K$^{-/+}$ lineage (Figure 15B). To confirm this finding, the fluorescence of HeLa cells containing amastigotes (20,000) were analysed by flow cytometry. The fluorescence intensity of the HeLa cells infected with IP6K$^{-/+}$ lineage was significantly lower than the control, suggesting that the disruption

of a single IP6K allele increases the multiplicative capacity of *T. cruzi* within the host-cell (Figure 15C).

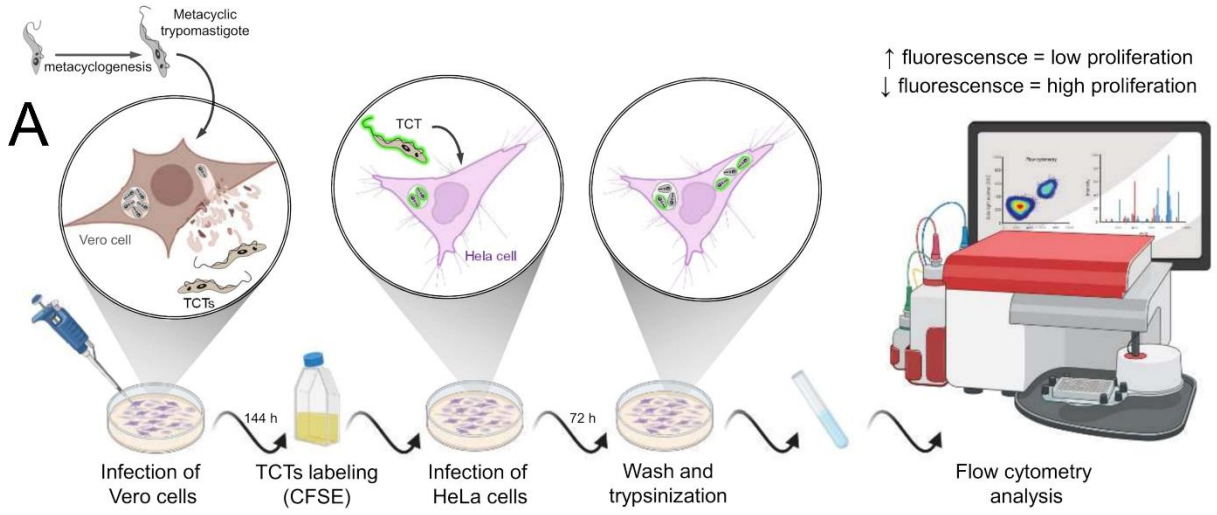

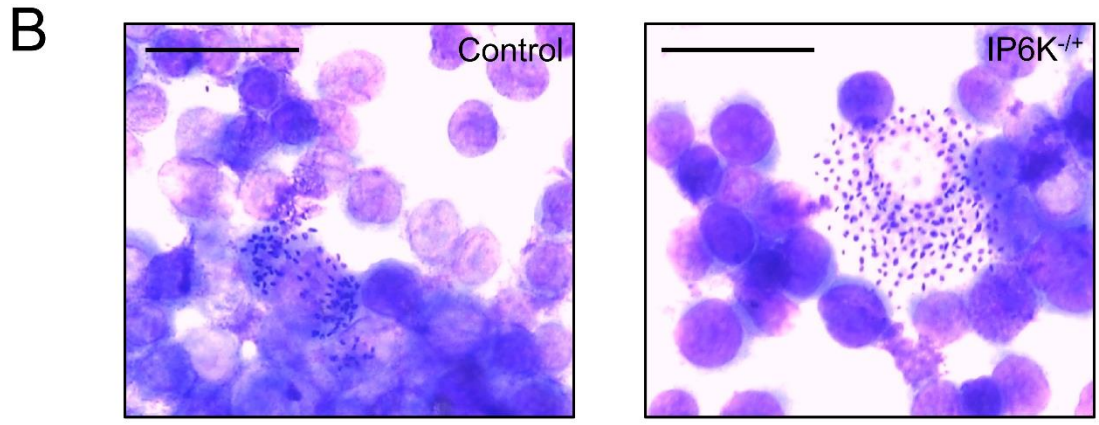

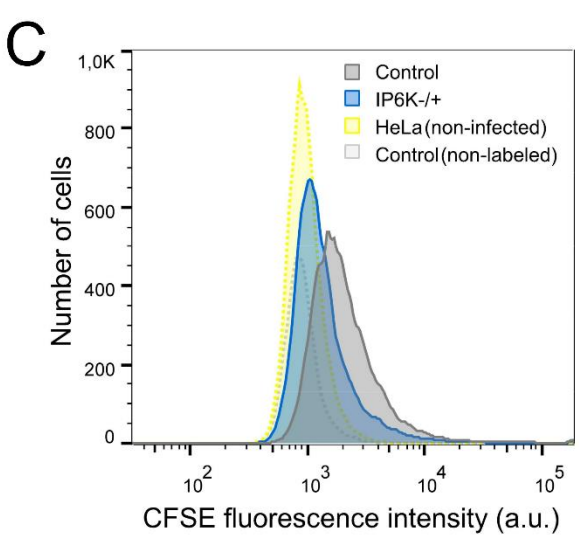

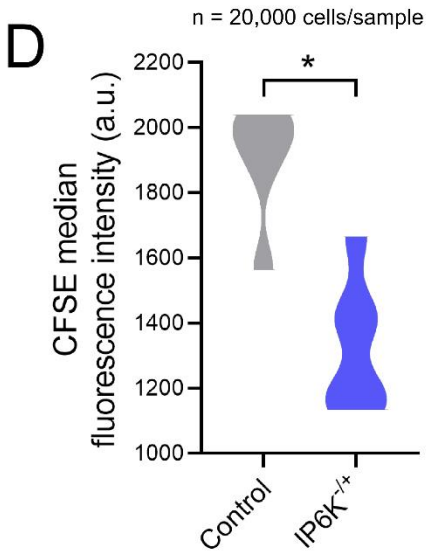

Figure 15. Results of the infection assays suggest that the trypomastigotes from *T. cruzi* IP6K$^{-/+}$ lineage have greater multiplicative capacity within the host cell. **A**. Scheme showing the main steps of the infection assay. **B**. Representative images evidencing the infected HeLa cells from the control and IP6K$^{-/+}$ groups. Bars = 50 µm. **C**. Overlapped histograms of the control (grey) and IP6K$^{-/+}$ (blue) groups analyzed by flow cytometry. The *T. cruzi* control group (non-labeled) and HeLa (non-infected) cells were used as controls (light gray and yellow, respectively). 20,000 cells were analyzed per sample in an assay performed in triplicate. **D**. Measurement of the CFSE median fluorescence intensity (a.u.) presented in C. The measurement was made using the FlowJo software. The violin plots were made from each replicate from an assay performed in quintuplicate. * = p< 0.05 using Student's t-test.

Interestingly, this finding suggests that IP6K (and most likely the PP-IPs) contributes to a low multiplicative capacity of *T. cruzi* within the host-cell, which contradicts the few existing data in the literature. For instance, IP_7 seems to be essential for the virulence and pathogenicity of *Cryptococcus neoformans* (Kang, 2018; Lev et al., 2015; Kang, 2018; Desmarini et al., 2020). In other words, our result seems to be paradoxical and generates a conundrum that we are still trying to understand.

However, we must not forget that this is just a preliminary assay and more data are needed to support the hypothesis that, perhaps, the depletion of a single IP6K allele leads to an increase in the number of infective forms (metacyclics) and, consequently, an increase in the proliferative capacity of *T. cruzi*. We intend to measure the number of metacyclics *T. cruzi* cells using α-gp82 antibody (Eickhoff, et al., 2010) (expressed exclusively in transitional and metacyclic forms of *T. cruzi*) to see if the data support this hypothesis.

5. CONCLUSIONS AND PERSPECTIVES FOR THE CONTINUATION OF THIS WORK

Taken together, our results suggest that IP6K is essential to *T. cruzi* epimastigotes and its disruption has harmful consequences for this parasite. The disruption of a single IP6K allele impairs normal cell growth, cell division and other metabolic pathways that have not yet been deeply studied, leading part of the *T. cruzi* cells to a possible dormant (quiescent) state. Paradoxically, apparently, the depletion of a single allele of IP6K also leads to *T. cruzi* being prone to multiplying further inside the host cell. Future assays will be made to determine whether IP6K is indeed essential for *T. cruzi* and its possible role in different metabolic pathways (including HR and DNA damage response), metacyclogenesis, and infectivity. Moreover, the PP-IPs levels will be verified in the generated lineages to confirm if the phenotypes observed are indeed due to decreased levels of IP_7. Furthermore, in collaboration with Dr. Noelia Lander (University of Cincinnati, USA), we are applying the CRISPR/Cas9-Riboswitch-Based method to conditionally downregulate the IP6K expression in *T. cruzi* and confirm its essentiality.

The expected results from these analyses will evidence if this kinase can be (or not) a potential target for the development of antiparasitic therapies. The hope that this kinase can be a good target for drug development is mainly for two reasons: First, IP6K has ~15% identity relative to its human homologs; second, kinases are excellent druggable targets (Naula et al., 2005) especially

in trypanosomatids, were G-protein-coupled receptors (the main targets used for drug development) are absent (Tagoe et al., 2015; Zdrazil et al., 2020).

6. DATA MANAGEMENT PLAN

Until the dissemination/publication of the results presented here, all data obtained are being stored in laboratory notebooks and on the institute's server (ncc.unesp.br/gridunesp/docs/), which requires personal access. Afterward, after publishing our data in a peer-reviewed scientific journal, we intend to make our raw data available in open access public repositories, such as GitHub (github.com/).

7. REFERENCES

Adl, S. M., Simpson, A. G. B., Lane, C. E., Lukeš, J., Bass, D., Bowser, S. S., et al. (2012). The revised classification of eukaryotes. *J. Eukaryot. Microbiol.* 59, 429–493. doi:10.1111/j.1550-7408.2012.00644.x.

Alexey, M. K., Diego, D., Tomáš, F., Benoit, M., Alexandros, S. (2019). RAxML-NG: a fast, scalable and user-friendly tool for maximum likelihood phylogenetic inference, Bioinformatics, Volume 35, Issue 21, 1 November 2019, Pages 4453–4455, doi.org/10.1093/bioinformatics/btz305.

Alves, C. L., Repolês, B. M., da Silva, M. S., Mendes, I. C., Marin, P. A., Aguiar, P. H. N., et al. (2018). The recombinase Rad51 plays a key role in events of genetic exchange in Trypanosoma cruzi. *Sci. Rep.* 8. doi:10.1038/s41598-018-31541-z.

Ananieva, E. A., Gillaspy, G. E., Ely, A., Burnette, R. N., & Erickson, F. L. (2008). Interaction of the WD40 domain of a myoinositol polyphosphate 5-phosphatase with SnRK1 links inositol, sugar, and stress signaling. Plant physiology, 148(4), 1868–1882. doi.org/10.1104/pp.108.130575.

Andrade, L. O., Machado, C. R. S., Chiari, E., Pena, S. D. J., and Macedo, A. M. (2002). Trypanosoma cruzi: role of host genetic background in the differential tissue distribution of parasite clonal populations. Exp. Parasitol. 100, 269–275. doi: 10.1016/S0014-4894(02)00024-3.

Bhandari, R., Chakraborty, A., & Snyder, S. H. (2007). Inositol pyrophosphate pyrotechnics. *Cell metabolism*, *5*(5), 321-323.

Barker, C. J., Wright, J., Hughes, P. J., Kirk, C. J., and Michell, R. H. (2004). Complex changes in cellular inositol phosphate complement accompany transit through the cell cycle. *Biochem. J.* doi:10.1042/BJ20031872.

Barker, C.J., Illies, C., Gaboardi, G.C. et al. (2009). Inositol pyrophosphates: structure, enzymology and function. Cell. Mol. Life Sci. 66, 3851. doi.org/10.1007/s00018-009-0115-2.

Beneke, T., Madden, R., Makin, L., Valli, J., Sunter, J., and Gluenz, E. (2017). A CRISPR Cas9 high-throughput genome editing toolkit for kinetoplastids. *R. Soc. Open Sci.* 4, 170095. doi:10.1098/rsos.170095.

Bennett, M., Onnebo, S. M., Azevedo, C., & Saiardi, A. (2006). Inositol pyrophosphates: metabolism and signaling. Cellular and molecular life sciences : CMLS, 63(5), 552–564. doi.org/10.1007/s00018-005-5446-z.

Bhandari, R., Saiardi, A., Ahmadibeni, Y., Snowman, A. M., Resnick, A. C., Kristiansen, T. Z., Molina,

H., Pandey, A., Werner, J. K., Jr., Juluri, K. R., Xu, Y., Prestwich, G. D., Parang, K., and Snyder, S. H. (2007). Protein pyrophosphorylation by inositol pyrophosphates is a posttranslational event. Proc Natl Acad Sci U S A 104, 15305–15310. doi.org/10.1073/pnas.0707338104.

Black, J. A., Crouch, K., Lemgruber, L., Lapsley, C., Dickens, N., Tosi, L. R., & McCulloch, R. (2020). *Trypanosoma brucei* ATR links DNA damage signaling during antigenic variation with regulation of RNA polymerase I-transcribed surface antigens. *Cell reports*, *30*(3), 836-851.

Brenière, S. F., Waleckx, E., and Barnabé, C. (2016). Over six thousand Trypanosoma cruzi strains classified into Discrete Typing Units (DTUs): attempt at an Inventory. PLoS Negl. Trop. Dis. 10:e0004792. doi: 10.1371/journal.pntd.0004792

Browne, A. J., Guerra, C. A., Alves, R. V., Da Costa, V. M., Wilson, A. L., Pigott, D. M., et al. (2017). The contemporary distribution of *Trypanosoma cruzi* infection in humans, alternative hosts and vectors. *Sci. Data* 4. doi:10.1038/sdata.2017.50.

Cerqueira, P. G., Passos-Silva, D. G., Vieira-da-Rocha, J. P., Mendes, I. C., de Oliveira, K. A., Oliveira, C. F. B., et al. (2017). Effect of ionizing radiation exposure on *Trypanosoma cruzi* ubiquitin-proteasome system. Mol. Biochem. Parasitol. 212, 55–67. doi: 10.1016/j.molbiopara.2017.01.005.

Cestari, I., and Stuart, K. (2015). Inositol phosphate pathway controls transcription of telomeric expression sites in trypanosomes. *Proc. Natl. Acad. Sci.* 112, E2803–E2812. doi:10.1073/pnas.1501206112.

Chakraborty, A. (2018), The inositol pyrophosphate pathway in health and diseases. Biol Rev, 93: 1203-1227. doi.org/10.1111/brv.12392.

Chakraborty, A., Kim, S., & Snyder, S. H. (2011). Inositol pyrophosphates as mammalian cell signals. Science signaling, 4(188), re1. doi.org/10.1126/scisignal.2001958.

Chamberlain, P. P., Qian, X., Stiles, A. R., Cho, J., Jones, D. H., Lesley, S. A., Grabau, E. A., Shears, S. B., & Spraggon, G. (2007). Integration of inositol phosphate signaling pathways via human ITPK1. The Journal of biological chemistry, 282(38), 28117–28125. doi.org/10.1074/jbc.M703121200.

Chang, H. H. Y., Pannunzio, N. R., Adachi, N., and Lieber, M. R. (2017). Non-homologous DNA end joining and alternative pathways to double-strand break repair. *Nat. Rev. Mol. Cell Biol.* 18, 495–506. doi:10.1038/nrm.2017.48.

Chiurillo, M. A., Moraes Barros, R. R., Souza, R. T., Marini, M. M., Antonio, C. R., Cortez, D. R., et al. (2016). Subtelomeric I-SceI-mediated double-strand breaks are repaired by homologous recombination in *Trypanosoma cruzi*. Front. Microbiol. 7:2041. doi: 10.3389/fmicb.2016.02041.

Choi, J. H., Williams, J., Cho, J., Falck, J. R., and Shears, S. B. (2007). Purification, sequencing, and molecular identification of a mammalian PP-InsP5kinase that is activated when cells are exposed to hyperosmotic stress. *J. Biol. Chem.* 282, 30763–30775. doi:10.1074/jbc.M704655200.

Claussin, C., and Chang, M. (2015). The many facets of homologous recombination at telomeres. *Microb. Cell* 2, 308–321. doi:10.15698/mic2015.09.224.

Cordeiro, C. D., Saiardi, A., and Docampo, R. (2017). The inositol pyrophosphate synthesis pathway in *Trypanosoma brucei* is linked to polyphosphate synthesis in acidocalcisomes. *Mol. Microbiol.* 106, 319–333. doi:10.1111/mmi.13766.

Costa, F. C., Francisco, A. F., Jayawardhana, S., Calderano, S. G., Lewis, M. D., Olmo, F., et al. (2018). Expanding the toolbox for *Trypanosoma cruzi*: A parasite line incorporating a

bioluminescence-fluorescence dual reporter and streamlined CRISPR/Cas9 functionality for rapid in vivo localisation and phenotyping. *PLoS Negl. Trop. Dis.* doi:10.1371/journal.pntd.0006388.

da Silva, M. S. (2021). DNA Double-Strand Breaks: A Double-Edged Sword for Trypanosomatids. *Front. Cell Dev. Biol.* doi:10.3389/fcell.2021.669041.

da Silva, M. S., and Cano, M. I. N. (2017). *Frontiers in Parasitology*. , eds. M. Santos da Silva and M. Isabel N. Cano BENTHAM SCIENCE PUBLISHERS doi:10.2174/9781681084053117010l.

da Silva, M. S., Cayres-Silva, G. R., Vitarelli, M. O., Marin, P. A., Hiraiwa, P. M., Araújo, C. B., et al. (2019). Transcription activity contributes to the firing of non-constitutive origins in African trypanosomes helping to maintain robustness in S-phase duration. *Sci. Rep.* 9, 18512. doi:10.1038/s41598-019-54366-w.

da Silva, M. S., Monteiro, J. P., Nunes, V. S., Vasconcelos, E. J., Perez, A. M., Freitas-Júnior, L. de H., et al. (2013). Leishmania amazonensis Promastigotes Present Two Distinct Modes of Nucleus and Kinetoplast Segregation during Cell Cycle. *PLoS One* 8, e81397. doi:10.1371/journal.pone.0081397.

da Silva, M. S., Muñoz, P. A. M., Armelin, H. A., and Elias, M. C. (2017). Differences in the Detection of BrdU/EdU Incorporation Assays Alter the Calculation for G1, S, and G2 Phases of the Cell Cycle in Trypanosomatids. *J. Eukaryot. Microbiol.* 64, 756–770. doi:10.1111/jeu.12408.

da Silva, M. S., Vitarelli, M. O., Souza, B. F., and Elias, M. C. (2020). Comparative Analysis of the Minimum Number of Replication Origins in Trypanosomatids and Yeasts. *Genes 2020,* Vol. 11, Page 523 11, 523. doi:10.3390/GENES11050523.

da Silveira, R. D. C. V., da Silva, M. S., Nunes, V. S., Perez, A. M., & Cano, M. I. N. (2013). The natural absence of RPA1N domain did not impair *Leishmania amazonensis* RPA-1 participation in DNA damage response and telomere protection. Parasitology, 140(4), 547-559.

Dean, S., Sunter, J. D., & Wheeler, R. J. (2016). TrypTag.org: A Trypanosome Genome-wide Protein Localisation Resource. Trends in parasitology, 33(2), 80–82. doi.org/10.1016/j.pt.2016.10.009

Dean, S., Sunter, J., Wheeler, R. J., Hodkinson, I., Gluenz, E., & Gull, K. (2015). A toolkit enabling efficient, scalable and reproducible gene tagging in trypanosomatids. Open biology, 5(1), 140197. doi.org/10.1098/rsob.140197

Deng, J., Yang, C., Wang, Y. et al. (2019). Inositol pyrophosphates mediated the apoptosis induced by hypoxic injury in bone marrow-derived mesenchymal stem cells by autophagy. Stem Cell Res Ther 10, 159. doi.org/10.1186/s13287-019-1256-3.

Draskovic, P., Saiardi, A., Bhandari, R., Burton, A., Ilc, G., Kovacevic, M., Snyder, S. H., & Podobnik, M. (2008). Inositol hexakisphosphate kinase products contain diphosphate and triphosphate groups. Chemistry & biology, 15(3), 274–286. doi.org/10.1016/j.chembiol.2008.01.011.

Du, F., Edwards, K., Shen, Z., Sun, B., De Lozanne, A., Briggs, S., & Firtel, R. A. (2008). Regulation of contractile vacuole formation and activity in Dictyostelium. The EMBO journal, 27(15), 2064–2076. doi.org/10.1038/emboj.2008.131.

Dyer, P., Dean, S., & Sunter, J. (2016). High-throughput Gene Tagging in Trypanosoma brucei. Journal of visualized experiments : JoVE, (114), 54342. doi.org/10.3791/54342

Edgar R. C. (2004). MUSCLE: multiple sequence alignment with high accuracy and high throughput. Nucleic acids research, 32(5), 1792–1797. doi.org/10.1093/nar/gkh340.

Eickhoff, C. S., Giddings, O. K., Yoshida, N., & Hoft, D. F. (2010). Immune responses to gp82 provide protection against mucosal *Trypanosoma cruzi* infection. Memórias do Instituto Oswaldo

Cruz, 105, 687-691.

El-Sayed, N. M. (2005). The Genome Sequence of Trypanosoma cruzi, Etiologic Agent of Chagas Disease. *Science (80-.).* 309, 409–415. doi:10.1126/science.1112631.

Endo-Streeter, S., Tsui, M. M., Odom, A. R., Block, J., & York, J. D. (2012). Structural studies and protein engineering of inositol phosphate multikinase. The Journal of biological chemistry, 287(42), 35360–35369. doi.org/10.1074/jbc.M112.365031.

Fridy, P.C., Otto, J.C., Dollins, D.E., York, J.D. (2007). Cloning and characterization of two human VIP1-like inositol hexakisphosphate and diphosphoinositol pentakisphosphate kinases. J Biol Chem. Oct 19;282(42):30754-62. doi: 10.1074/jbc.M704656200.

Garcia, J. B. F., da Rocha, J. P. V., Costa-Silva, H. M., Alves, C. L., MacHado, C. R., and Cruz, A. K. (2016). *Leishmania major* and *Trypanosoma cruzi* present distinct DNA damage responses. Mol. Biochem. Parasitol. 207, 23–32. doi: 10.1016/j.molbiopara.2016.05.004.

Gaunt, M. W., Yeo, M., Frame, I. A., and Stothard, J. R. (2003). Mechanism of genetic exchange in American trypanosomes. 421. doi:10.1038/nature01393.1.2.3.4.5.6.7.8.9.10.11.12.13.14.15.16.17.18.19.20.21.22.23.24.25. 26.Walther.

Gaunt, M. W., Yeo, M., Frame, I. A., Stothard, J. R., Carrasco, H. J., Taylor, M. C., et al. (2003). Mechanism of genetic exchange in American trypanosomes. Nature 421, 936–939. doi: 10.1038/nature01438.

Genois, M. M., Plourde, M., Éthier, C., Roy, G., Poirier, G. G., Ouellette, M., et al. (2015). Roles of Rad51 paralogs for promoting homologous recombination in *Leishmania infantum*. *Nucleic Acids Res.* 43, 2701–2715. doi:10.1093/nar/gkv118.

Glover L., Horn D., (2012). Trypanosomal histone γH2A and the DNA damage response. Molecular and Biochemical Parasitology, Volume 183, Issue 1, Pages 78-83, ISSN 0166-6851. doi:10.1016/j.molbiopara.2012.01.008.

Glover, L., McCulloch, R., & Horn, D. (2008). Sequence homology and microhomology dominate chromosomal double-strand break repair in African trypanosomes. Nucleic acids research, 36(8), 2608–2618. doi.org/10.1093/nar/gkn104.

Gómez-García, M. R., & Kornberg, A. (2004). Formation of an actin-like filament concurrent with the enzymatic synthesis of inorganic polyphosphate. Proceedings of the National Academy of Sciences of the United States of America, 101(45), 15876–15880. doi.org/10.1073/pnas.0406923101.

Holmes, W., & Jogl, G. (2006). Crystal structure of inositol phosphate multikinase 2 and implications for substrate specificity. The Journal of biological chemistry, 281(49), 38109–38116. doi.org/10.1074/jbc.M606883200.

Hortua Triana, M. A., Márquez-Nogueras, K. M., Chang, L., Stasic, A. J., Li, C., Spiegel, K. A., Sharma, A., Li, Z. H., & Moreno, S. N. J. (2018). Tagging of Weakly Expressed Toxoplasma gondii Calcium-Related Genes with High-Affinity Tags. The Journal of eukaryotic microbiology, 65(5), 709–721. doi.org/10.1111/jeu.12626

Hyun Ah Kang. (2018). Emerging roles of inositol pyrophosphates as key modulators of fungal pathogenicity, Virulence, 9:1, 563-565, DOI: 10.1080/21505594.2017.1421832.

Ivica Letunic (2021) Peer Bork, Interactive Tree Of Life (iTOL) v5: an online tool for phylogenetic tree display and annotation, Nucleic Acids Research, Volume 49. Issue W1. 2 July 2021. Pages W293–W296. doi.org/10.1093/nar/gkab301.

Jadav, R. S., Chanduri, M. V. L., Sengupta, S., and Bhandari, R. (2013). Inositol pyrophosphate synthesis by inositol hexakisphosphate kinase 1 is required for homologous recombination repair. *J. Biol. Chem.* 288, 3312–3321. doi:10.1074/jbc.M112.396556.

Jimenez, V., & Docampo, R. (2015). TcPho91 is a contractile vacuole phosphate sodium symporter that regulates phosphate and polyphosphate metabolism in *Trypanosoma cruzi*. Molecular microbiology, 97(5), 911–925. doi.org/10.1111/mmi.13075.

Khare, S., Nagle, A. S., Biggart, A., Lai, Y. H., Liang, F., Davis, L. C., et al. (2016). Proteasome inhibition for treatment of leishmaniasis, Chagas disease and sleeping sickness. *Nature* 537, 229–233. doi:10.1038/nature19339.

Khersonsky, O., & Tawfik, D. S. (2010). Enzyme promiscuity: a mechanistic and evolutionary perspective. Annual review of biochemistry, 79, 471–505. doi.org/10.1146/annurev-biochem-030409-143718.

Laffitte, M.-C. N., Leprohon, P., Papadopoulou, B., and Ouellette, M. (2016). Plasticity of the Leishmania genome leading to gene copy number variations and drug resistance. *F1000Research* 5, 2350. doi:10.12688/f1000research.9218.1.

Lander, N. and Chiurillo, M.A. (2019), State-of-the-art CRISPR/Cas9 Technology for Genome Editing in Trypanosomatids. J. Eukaryot. Microbiol., 66: 981-991. doi.org/10.1111/jeu.12747.

Lander, N., Li, Z. H., Niyogi, S., & Docampo, R. (2015). CRISPR/Cas9-Induced Disruption of Paraflagellar Rod Protein 1 and 2 Genes in Trypanosoma cruzi Reveals Their Role in Flagellar Attachment. mBio, 6(4), e01012. doi.org/10.1128/mBio.01012-15.

Lee, S., Kim, M.-G., Ahn, H., & Kim, S. (2020). Inositol Pyrophosphates: Signaling Molecules with Pleiotropic Actions in Mammals. Molecules, 25(9), 2208. MDPI AG. Retrieved from http://dx.doi.org/10.3390/molecules25092208.

Lev, S., Li, C., Desmarini, D., Saiardi, A., Fewings, N. L., Schibeci, S. D., et al. (2015). Fungal inositol pyrophosphate IP7 is crucial for metabolic adaptation to the host environment and pathogenicity. *MBio*. doi:10.1128/mBio.00531-15.

Lewis, M. D., Llewellyn, M. S., Yeo, M., Acosta, N., Gaunt, M. W., and Miles, M. A. (2011). Recent, independent and anthropogenic origins of *Trypanosoma cruzi* hybrids. PLoS Negl. Trop. Dis. 5:e1363. doi: 10.1371/journal.pntd.0001363.

Li, X., and Heyer, W.-D. (2008). Homologous recombination in DNA repair and DNA damage tolerance. *Cell Res.* 18, 99–113. doi:10.1038/cr.2008.1.

Machado, C. A., and Ayala, F. J. (2001). Nucleotide sequences provide evidence of genetic exchange among distantly related lineages of *Trypanosoma cruzi*. Proc. Natl. Acad. Sci. U.S.A. 98, 7396–7401. doi: 10.1073/pnas.121187198.

Malik, L. H., Singh, G. D., and Amsterdam, E. A. (2015). The epidemiology, clinical manifestations, and management of Chagas Heart disease. Clin. Cardiol. 38, 565–569. doi: 10.1002/clc.22421.

Mantilla, B. S., Amaral, L. D. Do, Jessen, H. J., and Docampo, R. (2021). The Inositol Pyrophosphate Biosynthetic Pathway of *Trypanosoma cruzi*. *ACS Chem. Biol.* doi:10.1021/acschembio.0c00759.

Mantilla, B. S., Kalesh, K., Brown, N. W., Jr, Fiedler, D., & Docampo, R. (2021). Affinity-based proteomics reveals novel targets of inositol pyrophosphate (5-IP_7)-dependent phosphorylation and binding in *Trypanosoma cruzi* replicative stages. Molecular microbiology, 115(5), 986–1004. doi.org/10.1111/mmi.14672.

Marcili, A., Lima, L., Cavazzana, M., Junqueira, A. C. V., Veludo, H. H., Maia Da Silva, F., et al.

(2009). A new genotype of *Trypanosoma cruzi* associated with bats evidenced by phylogenetic analyses using SSU rDNA, cytochrome b and histone H2B genes and genotyping based on ITS1 rDNA. Parasitology 136, 641–655. doi: 10.1017/S0031182009005861.

Marin, P. A., Da Silva, M. S., Pavani, R. S., Machado, C. R., and Elias, M. C. (2018). Recruitment kinetics of the homologous recombination pathway in procyclic forms of *Trypanosoma brucei* after ionizing radiation treatment. *Sci. Rep.* 8. doi:10.1038/s41598-018-23731-6.

Messenger, L. A., and Miles, M. A. (2015). Evidence and importance of genetic exchange among field populations of *Trypanosoma cruzi*. Acta Trop. 151, 150–155. doi: 10.1016/j.actatropica.2015.05.007.

Miller, G J, Wilson, M P, Majerus, P W, & Hurley, J H. (2005). Specificity determinants in inositol polyphosphate synthesis: Crystal structure of inositol 1,3,4-trisphosphate 5/6-kinase. United States. doi.org/10.1016/j.molcel.2005.03.016.

Mim, C., Cui, H., Gawronski-Salerno, J. A., Frost, A., Lyman, E., Voth, G. A., & Unger, V. M. (2012). Structural basis of membrane bending by the N-BAR protein endophilin. Cell, 149(1), 137–145. doi.org/10.1016/j.cell.2012.01.048.

Minini, M., Senni, A., Unfer, V., & Bizzarri, M. (2020). The Key Role of IP6K: A Novel Target for Anticancer Treatments?. Molecules (Basel, Switzerland), 25(19), 4401. doi.org/10.3390/molecules25194401.

Miranda, M. R., Sayé, M., Bouvier, L. A., Cámara, M.deL., Montserrat, J., & Pereira, C. A. (2012). Cationic amino acid uptake constitutes a metabolic regulation mechanism and occurs in the flagellar pocket of *Trypanosoma cruzi*. PloS one, 7(2), e32760. doi.org/10.1371/journal.pone.0032760.

Morrison, B. H., Bauer, J. A., Kalvakolanu, D. V., and Lindner, D. J. (2001). Inositol Hexakisphosphate Kinase 2 Mediates Growth Suppressive and Apoptotic Effects of Interferon-β in Ovarian Carcinoma Cells. *J. Biol. Chem.* 276, 24965–24970. doi:10.1074/jbc.M101161200.

Mukherjee, S., Haubner, J., &Chakraborty, A. (2020). Targeting the Inositol Pyrophosphate Biosynthetic Enzymes in Metabolic Diseases. Molecules, 25(6), 1403. MDPI AG. Retrieved from http://dx.doi.org/10.3390/molecules25061403.

Müller, L. S. M., Cosentino, R. O., Förstner, K. U., Guizetti, J., Wedel, C., Kaplan, N., et al. (2018). Genome organization and DNA accessibility control antigenic variation in trypanosomes. Nature 563, 121–125. doi: 10.1038/s41586-018-0619-8.

Myler, P., Nelson, R. G., Agabian, N., and Stuart, K. (1984a). Two mechanisms of expression of a predominant variant antigen gene of *Trypanosoma brucei*. Nature 309, 282–284. doi: 10.1038/309282a0.

Nagata, E., Luo, H. R., Saiardi, A., Bae, B. Il, Suzuki, N., and Snyder, S. H. (2005). Inositol hexakisphosphate kinase-2, a physiologic mediator of cell death. *J. Biol. Chem.* 280, 1634–1640. doi:10.1074/jbc.M409416200.

Naula, C., Parsons, M., and Mottram, J. C. (2005). Protein kinases as drug targets i1. Naula, C., Parsons, M. & Mottram, J. C. Protein kinases as drug targets in trypanosomes and Leishmania. in Biochimica et Biophysica Acta - Proteins and Proteomics 1754, 151–159 (2005).n trypanosomes and Leishmania. in *Biochimica et Biophysica Acta - Proteins and Proteomics*, 151–159. doi:10.1016/j.bbapap.2005.08.018.

Negreiros, R. S., Lander, N., Huang, G., Cordeiro, C. D., Smith, S. A., Morrissey, J. H., & Docampo, R. (2018). Inorganic polyphosphate interacts with nucleolar and glycosomal proteins in trypanosomatids. Molecular microbiology, 110(6), 973–994. doi.org/10.1111/mmi.14131.

Nenarokova, A., Záhonová, K., Krasilnikova, M., Gahura, O., McCulloch, R., Zíková, A., et al. (2019). Causes and Effects of Loss of Classical Nonhomologous End Joining Pathway in Parasitic Eukaryotes. *MBio* 10. doi:10.1128/mbio.01541-19.

Niyogi, S., Jimenez, V., Girard-Dias, W., de Souza, W., Miranda, K., & Docampo, R. (2015). Rab32 is essential for maintaining functional acidocalcisomes, and for growth and infectivity of *Trypanosoma cruzi*. Journal of cell science, 128(12), 2363–2373. doi.org/10.1242/jcs.169466.

Niyogi, S., Mucci, J., Campetella, O., & Docampo, R. (2014). Rab11 regulates trafficking of trans-sialidase to the plasma membrane through the contractile vacuole complex of *Trypanosoma cruzi.* PLoS pathogens, 10(6), e1004224. doi.org/10.1371/journal.ppat.1004224.

Pack, L. R., Daigh, L. H., & Meyer, T. (2019). Putting the brakes on the cell cycle: mechanisms of cellular growth arrest. Current opinion in cell biology, 60, 106–113. doi.org/10.1016/j.ceb.2019.05.005.

Passos-Silva, D. G., Rajão, M. A., Nascimento de Aguiar, P. H., Vieira-da-Rocha, J. P., Machado, C. R., and Furtado, C. (2010). Overview of DNA Repair in *Trypanosoma cruzi*, *Trypanosoma brucei*, and *Leishmania major*. *J. Nucleic Acids* 2010, 840768. doi:10.4061/2010/840768.

Pearson, W. R. (2013). An introduction to sequence similarity ("homology") searching. *Curr. Protoc. Bioinforma.* doi:10.1002/0471250953.bi0301s42.

Pedroso, A., Cupolillo, E., and Zingales, B. (2003). Evaluation of *Trypanosoma cruzi* hybrid stocks based on chromosomal size variation. Mol. Biochem. Parasitol. 129, 79–90. doi: 10.1016/S0166-6851(03)00096-3.

Pesesse, X., Choi, K., Zhang, T., and Shears, S. B. (2004). Signaling by higher inositol polyphosphates: Synthesis of bisdiphosphoinositol tetrakisphosphate ("InsP8") is selectively activated by hyperosmotic stress. *J. Biol. Chem.* 279, 43378–43381. doi:10.1074/jbc.C400286200.

Pfeiffer, P., Goedecke, W., and Obe, G. (2000). Mechanisms of DNA double-strand break repair and their potential to induce chromosomal aberrations. Mutagenesis 15, 289–302. doi: 10.1093/mutage/15.4.289.

Ramírez, J. D., and Llewellyn, M. S. (2014). Reproductive clonality in protozoan pathogens – truth or artefact? Mol. Ecol. 23, 4195–4202. doi: 10.1111/mec.12872.

Ramírez, J. D., Guhl, F., Messenger, L. A., Lewis, M. D., Montilla, M., Cucunuba, Z., et al. (2012). Contemporary cryptic sexuality in *Trypanosoma cruzi*. Mol. Ecol. 21, 4216–4226. doi: 10.1111/j.1365-294X.2012.05699.x.

Rao, F., Cha, J., Xu, J., Xu, R., Vandiver, M. S., Tyagi, R., et al. (2014). Inositol Pyrophosphates Mediate the DNA-PK/ATM-p53 Cell Death Pathway by Regulating CK2 Phosphorylation of Tti1/Tel2. *Mol. Cell*. doi:10.1016/j.molcel.2014.02.020.

Rao, F., Xu, J., Fu, C., Cha, J. Y., Gadalla, M. M., Xu, R., et al. (2015). Inositol pyrophosphates promote tumor growth and metastasis by antagonizing liver kinase B1. *Proc. Natl. Acad. Sci.* 112, 1773–1778. doi:10.1073/pnas.1424642112.

Regis-da-Silva, C. G., Freitas, J. M., Passos-Silva, D. G., Furtado, C., Augusto-Pinto, L., Pereira, M. T., et al. (2006). Characterization of the *Trypanosoma cruzi* Rad51 gene and its role in recombination events associated with the parasite resistance to ionizing radiation. *Mol. Biochem. Parasitol.* 149, 191–200. doi:10.1016/j.molbiopara.2006.05.012.

Reis-Cunha, J. L., Rodrigues-Luiz, G. F., Valdivia, H. O., Baptista, R. P., Mendes, T. A. O., de Morais, G. L., et al. (2015). Chromosomal copy number variation reveals differential levels of

genomic plasticity in distinct Trypanosoma cruzi strains. BMC Genomics 16:499. doi: 10.1186/s12864-015-1680-4.

Repolês, B. M., Machado, C. R., and Florentino, P. T. V. (2020). DNA lesions and repair in trypanosomatids infection. Genet. Mol. Biol. 43:e20190163. doi: 10.1590/1678-4685-GMB-2019-0163.

Resende, B. C., Oliveira, A. C. S., Guañabens, A. C. P., Repolês, B. M., Santana, V., Hiraiwa, P. M., et al. (2020). The Influence of Recombinational Processes to Induce Dormancy in *Trypanosoma cruzi*. *Front. Cell. Infect. Microbiol.* doi:10.3389/fcimb.2020.00005.

Saiardi, A., Bhandari, R., Resnick, A. C., Snowman, A. M., and Snyder, S. H. (2004). Phosphorylation of proteins by inositol pyrophosphates. *Science (80-.).* 306, 2101–2105. doi:10.1126/science.1103344.

Saiardi, A., Caffrey, J. J., Snyder, S. H., and Shears, S. B. (2000). The inositol hexakisphosphate kinase family. Catalytic flexibility and function in yeast vacuole biogenesis. *J. Biol. Chem.* 275, 24686–24692. doi:10.1074/jbc.M002750200.

Saiardi, A., Erdjument-Bromage, H., Snowman, A. M., Tempst, P., & Snyder, S. H. (1999). Synthesis of diphosphoinositol pentakisphosphate by a newly identified family of higher inositol polyphosphate kinases. Current biology : CB, 9(22), 1323–1326. doi.org/10.1016/s0960-9822(00)80055-x.

Saiardi, A., Resnick, A. C., Snowman, A. M., Wendland, B., & Snyder, S. H. (2005). Inositol pyrophosphates regulate cell death and telomere length through phosphoinositide 3-kinase-related protein kinases. Proceedings of the National Academy of Sciences of the United States of America, 102(6), 1911–1914. doi.org/10.1073/pnas.0409322102.

Saiardi, A., Sciambi, C., McCaffery, J. M., Wendland, B., & Snyder, S. H. (2002). Inositol pyrophosphates regulate endocytic trafficking. Proceedings of the National Academy of Sciences of the United States of America, 99(22), 14206–14211. doi.org/10.1073/pnas.212527899.

Salic, A., and Mitchison, T. J. (2008). A chemical method for fast and sensitive detection of DNA synthesis in vivo. *Proc. Natl. Acad. Sci. U. S. A.* 105, 2415–20. doi:10.1073/pnas.0712168105.

Salvador, C. G., José, M. S. M., Toni, G. (2009). trimAl: a tool for automated alignment trimming in large-scale phylogenetic analyses, Bioinformatics, Volume 25, Issue 15, 1 August 2009, Pages 1972–1973, doi.org/10.1093/bioinformatics/btp348.

Sánchez-Valdéz, F. J., Padilla, A., Wang, W., Orr, D., & Tarleton, R. L. (2018). Spontaneous dormancy protects *Trypanosoma cruzi* during extended drug exposure. Elife, 7, e34039.

Schwabl, P., Imamura, H., Van den Broeck, F., Costales, J. A., Maiguashca-Sánchez, J., Miles, M. A., et al. (2019). Meiotic sex in Chagas disease parasite *Trypanosoma cruzi*. *Nat. Commun.* doi:10.1038/s41467-019-11771-z.

Shah, A., Ganguli, S., Sen, J., and Bhandari, R. (2017). Inositol Pyrophosphates: Energetic, Omnipresent and Versatile Signalling Molecules. *J. Indian Inst. Sci.* doi:10.1007/s41745-016-0011-3.

Shaner, N. C., Lambert, G. G., Chammas, A., Ni, Y., Cranfill, P. J., Baird, M. A., Sell, B. R., Allen, J. R., Day, R. N., Israelsson, M., Davidson, M. W., & Wang, J. (2013). A bright monomeric green fluorescent protein derived from Branchiostoma lanceolatum. Nature methods, 10(5), 407–409. doi.org/10.1038/nmeth.2413

Shears S. B. (2004). How versatile are inositol phosphate kinases?. The Biochemical journal, 377(Pt

2), 265–280. doi.org/10.1042/BJ20031428.

Shears S. B. (2015). Inositol pyrophosphates: why so many phosphates?. Advances in biological regulation, 57, 203–216. doi.org/10.1016/j.jbior.2014.09.015.

Shears S. B. (2018). Intimate connections: Inositol pyrophosphates at the interface of metabolic regulation and cell signaling. Journal of cellular physiology, 233(3), 1897–1912. doi.org/10.1002/jcp.26017.

Shears, S.B., Baughman, B.M., Gu, C., Nair, V.S., Wang, H. (2017). The significance of the 1-kinase/1-phosphatase activities of the PPIP5K family. Adv Biol Regul. Jan;63:98-106. doi: 10.1016/j.jbior.2016.10.003.

Sievers, F., Wilm, A., Dineen, D., Gibson, T. J., Karplus, K., Li, W., Lopez, R., McWilliam, H., Remmert, M., Söding, J., Thompson, J. D., & Higgins, D. G. (2011). Fast, scalable generation of high-quality protein multiple sequence alignments using Clustal Omega. Molecular systems biology, 7, 539. doi.org/10.1038/msb.2011.75.

Sleigh M. J. (1976). The mechanism of DNA breakage by phleomycin in vitro. Nucleic acids research, 3(4), 891–901. doi:10.1093/nar/3.4.891.

Stanners, C. P., and Till, J. E. (1960). DNA synthesis in individual L-strain mouse cells. *Biochim. Biophys. Acta* 37, 406–19.

Stephens, L., Radenberg, T., Thiel, U., Vogel, G., Khoo, K. H., Dell, A., Jackson, T. R., Hawkins, P. T., & Mayr, G. W. (1993). The detection, purification, structural characterization, and metabolism of diphosphoinositol pentakisphosphate(s) and bisdiphosphoinositol tetrakisphosphate(s). The Journal of biological chemistry, 268(6), 4009–4015.

Stortz, J. A., Serafim, T. D., Alsford, S., Wilkes, J., Fernandez-Cortes, F., Hamilton, G., & McCulloch, R. (2017). Genome-wide and protein kinase-focused RNAi screens reveal conserved and novel damage response pathways in *Trypanosoma brucei*. *PLoS pathogens*, *13*(7), e1006477.

Sturm, N. R., Vargas, N. S., Westenberger, S. J., Zingales, B., and Campbell, D. A. (2003). Evidence for multiple hybrid groups in *Trypanosoma cruzi*. Int. J. Parasitol. 33, 269–279. doi: 10.1016/S0020-7519(02)00264-3.

Szijgyarto, Z., Garedew, A., Azevedo, C., & Saiardi, A. (2011). Influence of inositol pyrophosphates on cellular energy dynamics. Science (New York, N.Y.), 334(6057), 802–805. doi.org/10.1126/science.1211908.

Tagoe DNA, Kalejaiye TD, de Koning HP. The ever unfolding story of cAMP signaling in trypanosomatids: Vive la difference! Frontiers in Pharmacology. 2015.

Taylor, R., Jr, Chen, P. H., Chou, C. C., Patel, J., & Jin, S. V. (2012). KCS1 deletion in Saccharomyces cerevisiae leads to a defect in translocation of autophagic proteins and reduces autophagosome formation. Autophagy, 8(9), 1300–1311. doi.org/10.4161/auto.20681.

Tibayrenc, M., Kjellberg, F., and Ayala, F. J. (1990). A clonal theory of parasitic protozoa: the population structures of Entamoeba, Giardia, Leishmania, Naegleria, Plasmodium, Trichomonas, and Trypanosoma and their medical and taxonomical consequences. Proc. Natl. Acad. Sci. U.S.A. 87, 2414–2418. doi: 10.1073/pnas.87.7.2414.

Toettcher, J. E., Loewer, A., Ostheimer, G. J., Yaffe, M. B., Tidor, B., & Lahav, G. (2009). Distinct mechanisms act in concert to mediate cell cycle arrest. Proceedings of the National Academy of Sciences, 106(3), 785-790.

Ulrich, P. N., Jimenez, V., Park, M., Martins, V. P., Atwood, J., 3rd, Moles, K., Collins, D., Rohloff, P., Tarleton, R., Moreno, S. N., Orlando, R., & Docampo, R. (2011). Identification of contractile

vacuole proteins in *Trypanosoma cruzi*. PloS one, 6(3), e18013. doi.org/10.1371/journal.pone.0018013.

Ulrich, P. N., Lander, N., Kurup, S. P., Reiss, L., Brewer, J., Soares Medeiros, L. C., Miranda, K., & Docampo, R. (2014). The acidocalcisome vacuolar transporter chaperone 4 catalyzes the synthesis of polyphosphate in insect-stages of *Trypanosoma brucei* and *T. cruzi*. The Journal of eukaryotic microbiology, 61(2), 155–165. doi.org/10.1111/jeu.12093.

Urbina, J. A., and Docampo, R. (2003). Specific chemotherapy of Chagas disease: Controversies and advances. *Trends Parasitol.* 19, 495–501. doi:10.1016/j.pt.2003.09.001.

Voglmaier, S. M., Bembenek, M. E., Kaplin, A. I., Dormán, G., Olszewski, J. D., Prestwich, G. D., & Snyder, S. H. (1996). Purified inositol hexakisphosphate kinase is an ATP synthase: diphosphoinositol pentakisphosphate as a high-energy phosphate donor. Proceedings of the National Academy of Sciences of the United States of America, 93(9), 4305–4310. doi.org/10.1073/pnas.93.9.4305.

Wang, H., DeRose, E. F., London, R. E., & Shears, S. B. (2014). IP6K structure and the molecular determinants of catalytic specificity in an inositol phosphate kinase family. Nature communications, 5, 4178. doi.org/10.1038/ncomms5178.

Waterhouse, A. M., Procter, J. B., Martin, D. M. A., Clamp, M., Barton, G. J. (2009) Jalview Version 2-a multiple sequence alignment editor and analysis workbench. Bioinformatics 25: 1189-1191. doi:10.1093/bioinformatics/btp033

Williams, F. M. (1971). “Dynamics of microbial populations,” in *Systems analysis and simulation in ecology*, ed. B. C. Patten (New York: Academic Press Inc.), 198–268.

Wilson, M. S., Livermore, T. M., & Saiardi, A. (2013). Inositol pyrophosphates: between signalling and metabolism. *Biochemical Journal*, *452*(3), 369-379.

Wu, M., Chong, L. S., Perlman, D. H., Resnick, A. C., & Fiedler, D. (2016). Inositol polyphosphates intersect with signaling and metabolic networks via two distinct mechanisms. Proceedings of the National Academy of Sciences of the United States of America, 113(44), E6757–E6765. doi.org/10.1073/pnas.1606853113.

Wyman, C., and Kanaar, R. (2006). DNA Double-Strand Break Repair: All’s Well that Ends Well. *Annu. Rev. Genet.* 40, 363–383. doi:10.1146/annurev.genet.40.110405.090451.

Yang, X., & Shears, S. B. (2000). Multitasking in signal transduction by a promiscuous human Ins(3,4,5,6)P(4) 1-kinase/Ins(1,3,4)P(3) 5/6-kinase. The Biochemical journal, 351 Pt 3(Pt 3), 551–555.

Yeeles, J. T. P., Poli, J., Marians, K. J., and Pasero, P. (2013). Rescuing stalled or damaged replication forks. *Cold Spring Harb. Perspect. Biol.* 5. doi:10.1101/cshperspect.a012815.

Yonetani, Y., Hochegger, H., Sonoda, E., Shinya, S., Yoshikawa, H., Takeda, S., et al. (2005). Differential and collaborative actions of Rad51 paralog proteins in cellular response to DNA damage. Nucleic Acids Res. 33, 4544–4552. doi: 10.1093/nar/gki766.

Zdrazil B, Richter L, Brown N, Guha R. Moving targets in drug discovery. Sci Rep. 2020;

Zhang, W. W., & Matlashewski, G. (2015). CRISPR-Cas9-Mediated Genome Editing in Leishmania donovani. mBio, 6(4), e00861. doi.org/10.1128/mBio.00861-15.

Zhao, F., Kim, W., Kloeber, J. A., and Lou, Z. (2020). DNA end resection and its role in DNA replication and DSB repair choice in mammalian cells. Exp. Mol. Med. 52, 1705–1714. doi: 10.1038/s12276-020-00519-1.

Zingales, B., Miles, M. A., Campbell, D. A., Tibayrenc, M., Macedo, A. M., Teixeira, M. M. G., et al. (2012). The revised *Trypanosoma cruzi* subspecific nomenclature: rationale, epidemiological relevance and research applications. Infect. Genet. Evol. 12, 240–253. doi: 10.1016/j.meegid.2011.12.009.

Zingales, B., Pereira, M. E. S., Almeida, K. A., Umezawa, E. S., Nehme, N. S., Oliveira, R. P., et al. (1997). Biological Parameters and Molecular Markers of Clone CL Brener - The Reference Organism of the *Trypanosoma cruzi* Genome Project. *Mem. Inst. Oswaldo Cruz*. doi:10.1590/S0074-02761997000600016.

8. ACTIVITIES CARRIED OUT DURING THE DEVELOPMENT OF THE PROJECT

8.1 Participation in events with work presentation

- 30th Annual Molecular Parasitology & Vector Biology Symposium - Center for Tropical & Emerging Global Diseases - University of Georgia, Athens, GA.

The event took place online on May 4, 2021, the international event “30th Annual Molecular Parasitology & Vector Biology Symposium” – Center for Tropical & Emerging Global Diseases – University of Georgia, Athens, GA (ctegd.uga.edu/events/symposium/). In this symposium, I presented the work entitled “Generation of *T. cruzi* lineages knock-out for the kinase IP6K and evaluation of homologous recombination repair capacity: Preliminary analyses”, which was published in the event summary book (ctegd.uga.edu/files/2021/05/Book2021.pdf).

- XXXVI Annual Meeting of the Brazilian Society of Protozoology / XLVII Annual Meeting on Basic Research in Chagas Disease – Brazilian Society of Protozoology (SBPz).

The event took place between online on August 30 and September 1, 2021, the event “XXXVI Annual Meeting of the Brazilian Society of Protozoology / XLVII Annual Meeting on Basic Research in Chagas Disease” of the Brazilian Society of Protozoology (SBPZ). In this event, I presented the work entitled “Could the inositol pyrophosphates (PP-IPs) be involved in DNA repair pathways in the human pathogen *Trypanosoma cruzi?* Preliminary analyses”.

- Inositol Phosphates Annual Meeting based on research about inositol phosphates and pyrophosphates

This event took place online on a Zoom Meeting between Monday, January 10th 2022 and Wednesday, January 12th 2022. During this event, “Inositol Phosphates 2022 Even more the merrier.”, I explored other scientific works presented by the Inositol Phosphates and Pyrophosphates theme whence my networking and attendee information can be found here: www.inositolphosphates.org/networking Details about the meeting can be found here: www.inositolphosphates.org/

- WorldLeish7 (WL7), 7th World Congress on Leishmaniasis – Cartagena de Indes, Colombia.

The event took place on the 1st to 6th August, 2022, the international event “7th World Congress on Leishmaniasis” in Cartagena de Indes, Colombia (https://www.worldleish7.org/). In this symposium, I presented the work entitled “Depletion of a single IP6K allele alters cell morphology and lead part of the *Trypanosoma cruzi* population to dormancy”, which was awarded a certificate (https://www.worldleish7.org/certificates/). *A disclaimer was given that the WL7 webpage would stop functioning in March 2023.

8.2 Articles published

1. Abuchery, B.E., Black, J.A., and da Silva, M.S. (2021) Single-cell transcriptomics reveals hidden information in trypanosomatids. *Trends in parasitology*. 38(1), 4-6. DOI: 10.1016/j.pt.2021.10.006

2. Assis, L.H., Andrade-Silva, D., Shiburah, M.E., de Oliveira, B.C., Paiva, S.C., Abuchery, B. E., Ferri, Y.G., Fontes, V.S., da Silva, L.S., da Silva, M.S., and Cano, M.I.N. (2021) Cell Cycle, Telomeres, and Telomerase in *Leishmania* spp.: What Do We Know So Far? *Cells*, 10(11), 3195. DOI: 10.3390/cells10113195